

Response of the NCAR Climate System Model to Increased CO₂ and the Role of Physical Processes

GERALD A. MEEHL, WILLIAM D. COLLINS, BYRON A. BOVILLE, JEFFREY T. KIEHL, T. M. L. WIGLEY, AND JULIE M. ARBLASTER

National Center for Atmospheric Research, Boulder, Colorado*

(Manuscript received 4 December 1998, in final form 26 May 1999)

ABSTRACT

The global warming resulting from increased CO₂ is addressed in the context of two regional processes that contribute to climate change in coupled climate models, the “El Niño-like” response (slackening of the equatorial Pacific SST gradient) and sea-ice response at high latitudes. The National Center for Atmospheric Research (NCAR) Climate System Model (CSM) response is compared with results from a coupled model that produces comparatively greater global warming, the NCAR U.S. Department of Energy (DOE) global coupled model. In an experiment where atmospheric CO₂ is increased 1% yr⁻¹ compound, globally averaged surface air temperature increase near the time of CO₂ doubling for the CSM is 1.43°C (3.50°C for the DOE model). Analysis of a simple coupled model shows the CSM equilibrium sensitivity to doubled CO₂ is comparable to that from the slab ocean version (about 2.1°C). One process that contributes to global warming (estimated to be about 5% in one slab ocean model), as well as to significant Pacific region climate effects, is the El Niño-like response. It is a notable feature in the DOE model and some other global coupled models but does not occur in the CSM. The authors show that cloud responses are a major determining factor. With increased CO₂, there are negative net cloud-forcing differences in the western equatorial Pacific in the CSM and DOE models, but large positive differences in the DOE model and negative differences in the CSM in the eastern equatorial Pacific. This produces asymmetric cloud radiative forcing contributing to an El Niño-like response in the DOE model and not in the CSM. To remove the amplifying effects of ocean dynamics and to identify possible parameter-dependent processes that could contribute to such cloud forcing changes, the authors analyze slab ocean versions of the coupled models in comparison with a slab ocean configuration of the atmospheric model in the CSM [Community Climate Model Version 3 (CCM3)] that includes prognostic cloud liquid water. The latter shows a change in sign (from negative to positive) of the net cloud forcing in the eastern equatorial Pacific with doubled CO₂, similar to the DOE model, in comparison with the CCM3 version with diagnostic cloud liquid water. Atmospheric Model Intercomparison Project (prescribed SST) experiments show that all three atmospheric models (DOE, CCM3 with diagnostic cloud liquid water, and CCM3 with prognostic cloud liquid water) perform poorly relative to observations in terms of cloud radiative forcing, though CCM3 with prognostic cloud liquid water is slightly superior to the others. Another process that contributes to climate response to increasing CO₂ is sea-ice changes, which are estimated to enhance global warming by roughly 20% in the CSM and 37% in the DOE model. Sea-ice retreat with increasing CO₂ in the CSM is less than in the DOE model in spite of identical sea-ice formulations. Results from the North Atlantic and Greenland-Iceland-Norwegian (GIN) Sea region show that the surface energy budget response is controlled primarily by surface albedo (related to ice area changes) and cloud changes. However, a more important factor is the poleward ocean heat transport associated with changes in meridional overturning in the GIN Sea. With increased CO₂, the transport of warmer water from the south into this region in the DOE model is greater in comparison with that of the CSM. This leads to a larger ice reduction in the DOE model, thus also contributing to the enhanced contribution from ice albedo feedback in the DOE model in comparison with the CSM.

1. Introduction

A number of physical processes (e.g., clouds, water vapor, ice-snow albedo feedback, etc.) have been iden-

tified in previous global coupled model experiments that appear to contribute to the magnitude of the climate system response to an increase of CO₂ as reported by the Intergovernmental Panel on Climate Change (IPCC) (Kattenberg et al. 1996). Among these is a so-called El Niño-like response in the Pacific (Meehl and Washington 1996, hereinafter MW96; Knutson and Manabe 1998; Timmermann et al. 1999) characterized by greater warming of SSTs in the eastern tropical Pacific compared to the western Pacific. Because warm events in the eastern tropical Pacific are correlated with global mean warmth (Jones 1988), one can speculate that the

* The National Center for Atmospheric Research is sponsored by the National Science Foundation.

Corresponding author address: Dr. Gerald A. Meehl, NCAR/CGD, P.O. Box 3000, Boulder, CO 80307-3000.
E-mail: meehl@ncar.ucar.edu

El Niño-like response of some GCMs might enhance their global warming relative to models that do not have this response pattern.

Another positive feedback contributing to climate sensitivity is sea-ice response. As the climate warms from increasing CO₂, sea ice melts back, thus exposing more ocean with lower albedo. This increased water surface absorbs more solar radiation in summer, resulting in warmer SSTs at the ice edge, less sea ice forming in winter, more open ocean, and so on. The shrinking ice area contributes to decreased global albedo and further warming of the climate system.

Because the true sensitivity (defined as the equilibrium globally averaged surface temperature change with a doubling of CO₂) of the observed climate system is unknown, we have collections of model experiments such as those published by the IPCC (e.g., Kattenberg et al. 1996) that give us some impression of what the climate sensitivity might be (usually using atmospheric GCMs coupled to nondynamic slab ocean models). However, the models give a wide range of sensitivities, and those equilibrium sensitivities may not be related directly to a transient response in a coupled model. It is therefore of interest to identify the relative roles of different processes that could contribute to climate system response to a change in external forcing in different models. Thus, the purpose of this paper, in addition to documenting the basic National Center for Atmospheric Research (NCAR) Climate System Model (CSM) response to increasing CO₂, is to examine the globally averaged response and the role of two regional physical processes, the El Niño-like response and sea-ice response. Their roles will be explored in two models that have widely differing implied sensitivities (as derived from equilibrium slab ocean versions): the lower-sensitivity NCAR CSM and the higher-sensitivity NCAR Department of Energy (DOE) model. Both are fully coupled ocean-atmosphere-sea ice global climate models. It has been postulated that a coupled El Niño-like response in the tropical Pacific (MW96), and a strong sea ice response at high latitudes (Washington and Meehl 1996, hereinafter WM96) contribute to greater global warming in the DOE model. Associated processes will be compared between the DOE model and the CSM to explore their respective contributions to each model's climate response. Slab ocean versions of the coupled models are also analyzed to help identify model responses in the absence of the amplifying affects of ocean dynamics, as well as to compare possible parameterization-dependent aspects of the simulations particularly in regard to cloud liquid water.

2. The models

The NCAR CSM is a global coupled ocean-atmosphere-sea ice-land surface model (Boville and Gent 1998). The atmospheric component is the NCAR Community Climate Model version 3 (CCM3) with T42 res-

olution (roughly 2.5° × 2.5°) and 18 levels in hybrid coordinates (Kiehl et al. 1998). The global ocean GCM is nominally 2.4° × 2.4° reduced to 1.2° in latitude in the equatorial tropics, with 45 levels in the vertical (Gent et al. 1998). The sea ice component is adapted from the formulation in the NCAR DOE global coupled model (Meehl and Washington 1995; WM96), with Flato-Hibler ice dynamics and Semtner three-layer thermodynamics (Weatherly et al. 1998). The land surface model includes vegetation types and many surface processes (Bonan 1998). The CSM uses an accelerated deep ocean spinup procedure (which provides the initial state for the coupled model), does not use flux adjustment, and has little drift in the global mean surface air temperature for the duration of a 300-yr control run with no statistically significant regional trends in surface temperature [for full description see Boville and Gent (1998)]. The CSM also has been run with a 1% yr⁻¹ compound increase of CO₂ out to the time of CO₂ tripling near year 125 (Maruyama et al. 1997). The first part of that experiment (the integration run to the time of CO₂ doubling near year 70) will be analyzed here.

The NCAR DOE model has an R15 (roughly 4.5° lat × 7.5° long) 9-L atmosphere, a 1° × 1° 20-L global ocean model, and the same dynamic-thermodynamic sea ice model as in the CSM [Meehl and Washington (1995); WM96. Note that this is an early version of a subsequent DOE model, with different components, called the Parallel Climate Model (PCM) as described by Washington et al. (2000)]. The model uses an initialization spinup from the observed ocean state (Levitus 1982) and does not use flux adjustment. The globally averaged surface temperatures warm several tenths of a degree in the first 100 yr or so (the time period included in the submission to the Coupled Model Intercomparison Project) and cool several tenths in the last 35 yr so that over the entire duration of the 135-yr control run there is little net drift of globally averaged surface air temperature or consistent regional trends (e.g., Meehl et al. 2000). Meehl (1997) describes details of the spinup and systematic errors. The model has been used in a number of sensitivity experiments including a 1% yr⁻¹ compound CO₂ increase experiment (MW96) that will be analyzed further here, sensitivity experiments that include direct and indirect effects of sulfate aerosols (Meehl et al. 1996), and twentieth- and twenty-first-century climate experiments (Meehl et al. 2000).

The slab ocean model coupled to the atmospheric model (NCAR CCM3) is described in detail in Kiehl et al. (1996). It uses monthly mean spatially specified mixed layer depths and ocean heat transports (sometimes referred to as "Q flux"). The monthly mean ocean heat transports are determined from a simulation of the CCM3 forced with climatological SSTs. Using the model net surface heat flux and the observed SSTs, the implied ocean heat transport was determined. Thus the SST distribution is close to the observed. The model also employs a simple thermodynamic sea ice model, with

specified heat fluxes at the base of the ice. These heat fluxes were specified for the Arctic and Antarctic to yield realistic sea ice extent. The slab ocean version of the DOE model is described by Washington and Meehl (1993). Note that both slab ocean model versions have simple thermodynamic sea ice formulations and thus are different from the dynamic–thermodynamic ice models in the fully coupled versions.

3. Global-scale response in CO₂ increase experiments

Simulation of climate change using an idealized forcing scenario with CO₂ increasing at a rate of 1% yr⁻¹ compound has become a standard experiment to assess the response characteristics of coupled climate models (e.g., Meehl et al. 1997). Results from such experiments have shown a wide range of model responses by the IPCC (Kattenberg et al. 1996). For the NCAR CSM, the 20-yr average (years 60–79) globally averaged surface air temperature difference around the time of CO₂ doubling at year 70 is 1.43°C (Fig. 1a), with an increase of globally averaged precipitation of 2.0%. This can be compared to an equilibrium doubled-CO₂ experiment with the atmospheric model coupled to a slab mixed layer ocean with a globally averaged temperature increase of 2.08°C and precipitation increase of 3.9%. An analysis of a simple coupled climate model (see appendix) shows that if the CSM were run to equilibrium with doubled CO₂, its globally averaged surface air temperature response would be about 2.1°C, comparable to the sensitivity in the slab ocean equilibrium version. Thus the slab ocean version provides a good estimate of the sensitivity of the CSM in spite of the differences in sea ice and other formulations noted in the previous section.

Compared to the models listed by the IPCC (Kattenberg et al. 1996), the CSM is near the low end of climate model response to increased CO₂. Meanwhile, the NCAR DOE model shows the largest response of the models assessed by the IPCC (Kattenberg et al. 1996). Meehl et al. (1996) report that the 20-yr global average temperature change near the time of CO₂ doubling (years 56–75 where CO₂ doubles at around year 70; the transient experiment was run a total of 75 yr) is 3.50°C with a change in globally averaged precipitation of 3.1%. (Note that a shorter averaging period, years 65–74, yields a globally averaged temperature change of 3.8°C as reported by WM96, and by Kattenberg et al. 1996.) The doubled-CO₂ equilibrium temperature change from a slab ocean version is 4.58°C with an increase of globally averaged precipitation of 4.0%.

Surface temperature differences from the CSM in Figs. 1b and 1c show greatest warming in the winter hemisphere at high latitudes, particularly in the Northern Hemisphere during December–February (DJF; Fig. 1b). This feature, as well as less warming over the southern oceans year-round due to deep mixing there, is consistent with other global coupled models that have been

assessed by IPCC (Kattenberg et al. 1996). Similar results at high latitudes but with greater amplitude are evident for the DOE model (e.g., WM96; Meehl et al. 1996, 2000). The two models, however, show quite different temperature response patterns in the Pacific. The DOE model shows greater warming of SSTs in the equatorial eastern Pacific compared to the western Pacific, the El Niño–like pattern (MW96, their Fig. 2a), whereas there is almost uniform warming across the tropical Pacific in the CSM (Fig. 1).

Zonal mean temperature differences for CO₂ increase minus control are shown in Fig. 2a for DJF, and Fig. 2b for JJA. The enhanced warming at high latitudes at the surface in Figs. 1b,c is seen to be confined mostly to the lower troposphere in the winter hemisphere associated with reduced ice and snow extent. There is also a maximum warming in the upper tropical troposphere of greater than 2°C and cooling in the stratosphere. Similar features have been documented in other models assessed by the IPCC (Kattenberg et al. 1996).

Precipitation changes for the CSM in Fig. 3 show increases of precipitation in both seasons in many regions of the Tropics with smaller and more heterogeneous changes in other regions. In the Tropics, the pattern of precipitation change is more uniform than in the DOE model (MW96, their Fig. 3a), which shows an El Niño–like pattern of precipitation change in the tropical Pacific with greatest increases in the central and eastern Pacific and only small increases or decreases in the Australasian region. The Indian summer monsoon, as represented by precipitation averaged over land points in the region 5°–40°N, 60°–100°E for the JJA season increases by 11.6% in the CSM and by 1.4% in the DOE model. The enhancement of monsoon precipitation by an amount much larger than the global mean enhancement (e.g., Meehl and Washington 1993; Kitoh et al. 1997; Kattenberg et al. 1996) is partly due to the land heating faster than the ocean thus increasing land–sea temperature contrast. The relatively smaller increase in the DOE model is apparently related to the large-scale aspects of the El Niño–like response in precipitation which tends to suppress precipitation increases over south Asia, which is in turn associated with changes in the large-scale east–west atmospheric circulation (Meehl et al. 1996).

To illustrate the relative warming of land and ocean in the CSM, annual mean warming for the 20-yr period noted above near the time of CO₂ doubling for Northern Hemisphere land areas is +4.15°C, while Northern Hemisphere ocean areas warm by only +1.27°C. Southern Hemisphere land warms +1.59°C, and Southern Hemisphere ocean warms +0.93°C. For the DOE model, the comparable numbers are 4.85°C for Northern Hemisphere land areas, 3.01°C for Northern Hemisphere ocean areas, 4.10°C for Southern Hemisphere land, and 2.76°C for Southern Hemisphere ocean. As noted by Murphy (1995) and seen here, this differential land–ocean warming reflects two factors, a larger climate re-

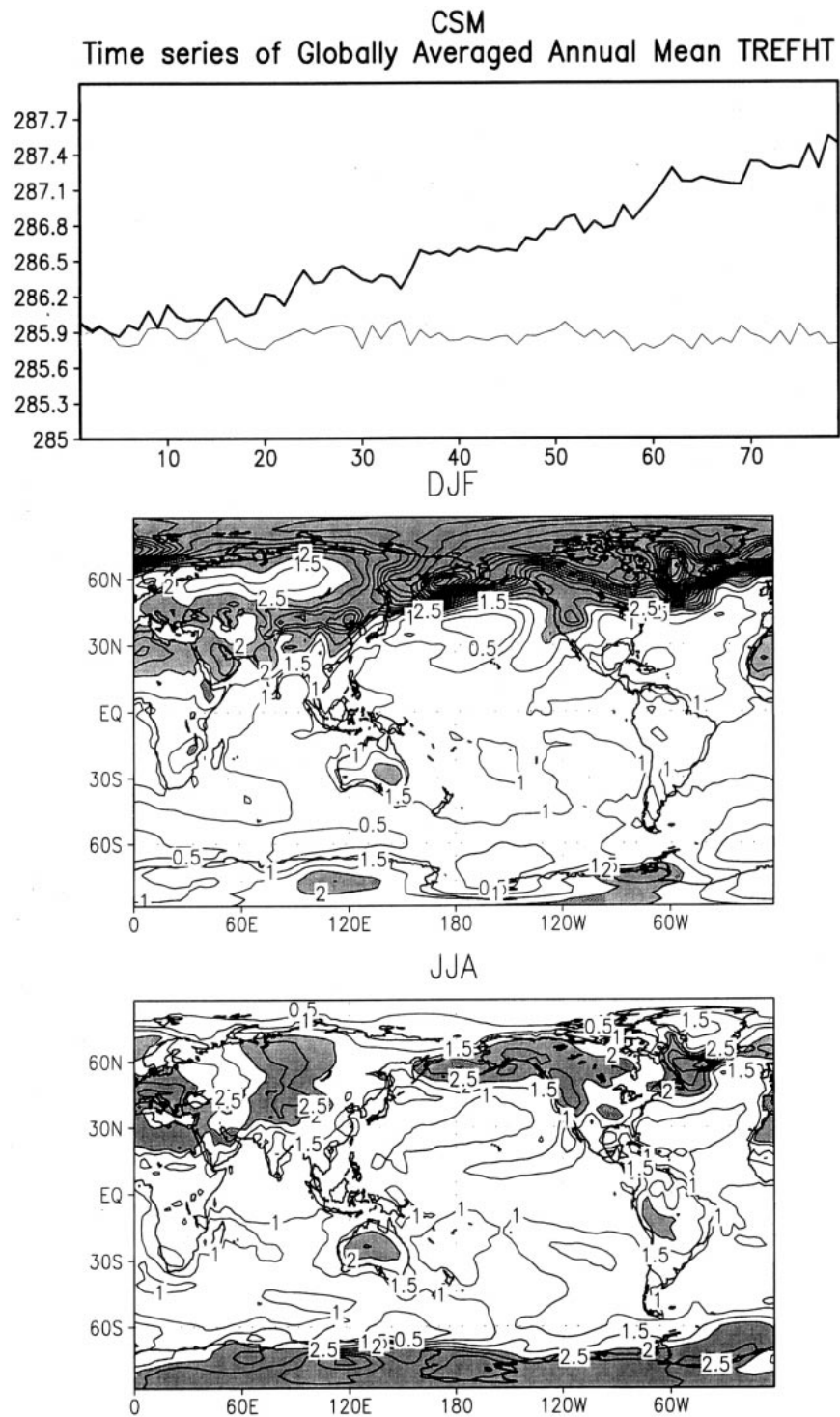


FIG. 1. (a) Time series of annual mean globally averaged surface air temperature [temperature at reference height (TREFHT)] for the NCAR CSM for control and 1% compound CO_2 increase experiment. CO_2 doubles at around year 70; (b) seasonal average, Dec–Jan–Feb (DJF), for surface air temperature (TREFHT) differences, transient CO_2 increase minus control, 20-yr average (years 60–79) around the time of CO_2 doubling; contour interval is 0.5°C ; areas greater than $+2.0^\circ\text{C}$ are shaded; (c) same as (b) except for Jun–Aug (JJA).

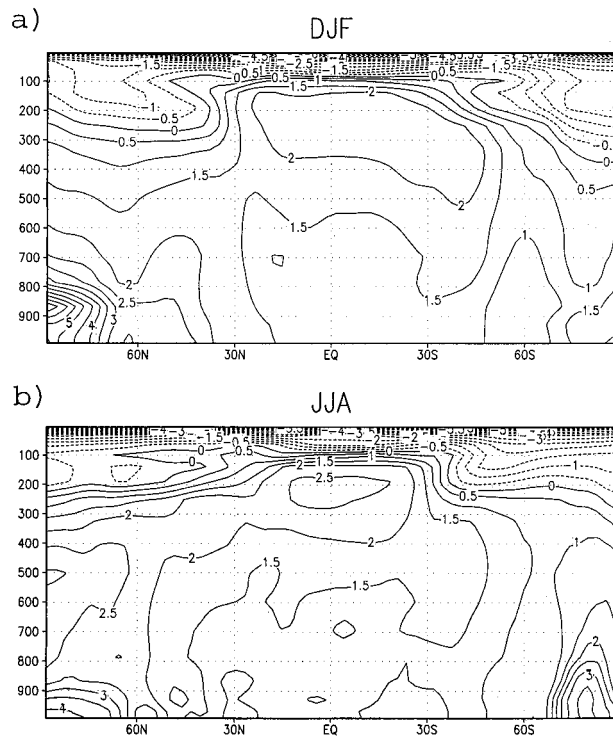


FIG. 2. (a) Seasonal average, DJF, zonal mean cross-section temperature differences ($^{\circ}\text{C}$), transient CO_2 increase minus control, 20-yr average (years 60–79) around the time of CO_2 doubling for the NCAR CSM; (b) same as (a) except for JJA. Contour interval is 0.5°C ; solid are positive, negative dashed.

sponse over land and a smaller lag over land due to lower thermal inertia.

The globally averaged changes of surface energy balance are shown at the top of Table 1, and globally averaged cloud forcing changes are shown at the top of Table 2. Both the CSM and DOE models show small decreases in sensible heat flux (less than 1 W m^{-2}), decreases in net infrared at the surface, and increases in latent heat flux. These changes are consistent with a warming of the surface temperature in each model. However, the greater magnitude global warming in the DOE model is associated with an increase ($+3.89 \text{ W m}^{-2}$) in absorbed solar radiation at the surface compared to a decrease of (-0.79 W m^{-2}) for the CSM. Both models have a decrease of sea ice area which would contribute to a global increase of absorbed solar, as will be discussed in detail shortly. However, the sign of the change in net cloud radiative forcing is different in the two models, with the CSM showing cloud forcing to be a negative feedback (-1.00 W m^{-2} in Table 2), but a positive feedback in the DOE model ($+3.86 \text{ W m}^{-2}$). The main contributor to this change in cloud feedback is reflected in the opposition in sign of the cloud shortwave forcing ($+4.73 \text{ W m}^{-2}$ for DOE, and -0.70 W m^{-2} for CSM). This difference, with obvious implications for the magnitude of global warming response in the coupled models, is an uncertainty that exists in other

models as well (e.g., Cess et al. 1996) with no clear guidance at present concerning which is correct. These changes in cloud forcing between the models are illustrated in the regional El Niño-like response discussed next.

4. Response in the tropical Pacific

For the CSM, Figs. 1b and 1c show surface temperature increases of around 1°C uniformly distributed across the equatorial Pacific. In contrast, the DOE coupled model (MW96) as well as a number of other global coupled models (Knutson and Manabe 1995, 1998; Tett 1995; Timmermann et al. 1999; Collins 2000) show a decrease of west–east temperature gradient (i.e., an El Niño-like response) to increasing CO_2 . In the observations, globally averaged temperatures are warmer during an El Niño event (Jones 1988; Nicholls et al. 1992). It is possible, therefore, that such a response in the Pacific due to increasing CO_2 contributes to enhanced global climate sensitivity (MW96). To help quantify such a contribution, an El Niño-like response was superimposed in an earlier slab ocean version of the DOE model (Meehl et al. 1993). In the $2 \times \text{CO}_2$ integration, the equatorial Pacific was specified to be 1.1°C warmer than the western equatorial Pacific, comparable to the relative SST difference across the Pacific for the DOE global coupled model (in Table 2, the warming in the eastern Pacific area is about 1°C greater than in the west). In the slab model, the doubled CO_2 experiment with the induced El Niño-like response warmed 5% more than the doubled CO_2 experiment without the El Niño-like response. Applied to the present coupled DOE model, that would mean that without the El Niño-like response, the warming could be estimated to be about 3.3° instead of 3.5°C . This can only be considered an approximate contribution since the estimate was derived from a mixed layer model version. However, it does demonstrate that there is a contribution to increasing global climate sensitivity in addition to the obvious regional implications for an El Niño-like response SST pattern in the Pacific (e.g., Meehl 1996).

Here we compare results from the NCAR DOE global coupled model with the CSM to explore reasons for the difference between the two models related to why the DOE model shows an El Niño-like response and the CSM does not. First, the base-state SSTs could affect such a response. The CSM has nearly the correct west–east SST gradient, but SSTs are less than observed by about 1.5°C (Meehl and Arblaster 1998). The DOE model also simulates roughly the correct SST gradient, but with SSTs higher than observed by about 1.5°C (MW96). Additionally, the cloud responses discussed below contribute to the SST changes (Chou et al. 1998), and the base-state SSTs themselves are a function of those cloud processes. Therefore, coupled responses of the climate system in the tropical Pacific must be an-

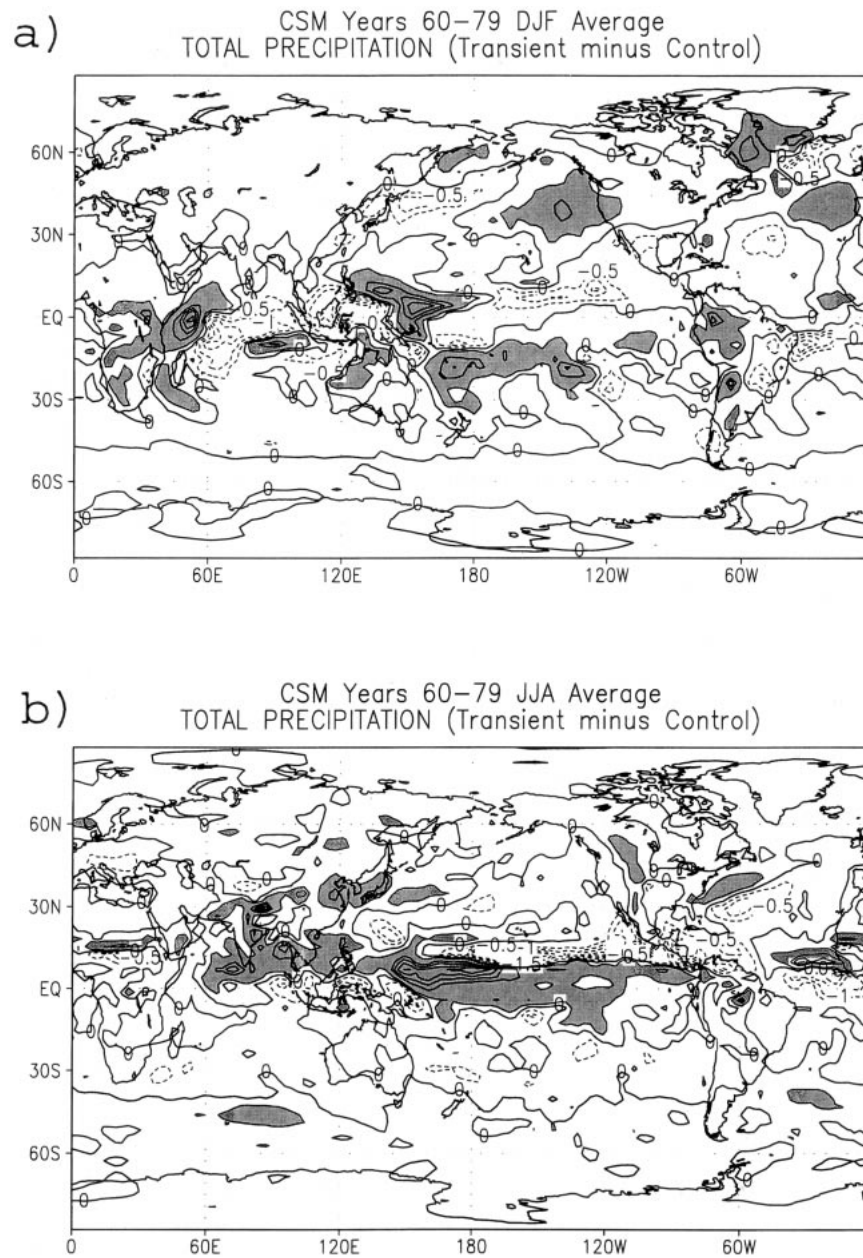


FIG. 3. (a) Seasonal average, DJF, precipitation differences, transient CO_2 increase minus control, 20-yr average (years 60–79) around the time of CO_2 doubling for the NCAR CSM; contour interval is 0.5 mm day^{-1} ; areas of precipitation increase greater than $+0.5 \text{ mm day}^{-1}$ are shaded; (b) same as (a) except JJA.

alyzed to determine the relative contributions to the El Niño-like response or lack thereof.

In Table 1 for the DOE model, as noted above, there is a pronounced El Niño-like response to increased CO_2 , with the eastern Pacific warming about 1°C more than in the west ($+3.23^\circ$ vs $+2.27^\circ\text{C}$). In the CSM there is little evidence of this El Niño-like response; the warming in the eastern and western Pacific is nearly the same ($+1.07^\circ$ vs $+1.11^\circ\text{C}$, respectively, as also noted in Fig. 1). Note that in the DOE model, this slackening

of the west–east SST gradient occurs as a trend throughout the increased CO_2 experiment (MW96, their Fig. 2b).

MW96 provide evidence that regionally specific forcing changes and consequent coupled ocean–atmosphere responses are linked to the El Niño-like response. Overall, the DOE model shows strongly asymmetric net cloud forcing changes across the Pacific (Table 2) with -5.47 W m^{-2} in the west and $+7.61 \text{ W m}^{-2}$ in the east (this means roughly 5 W m^{-2} less energy enters the

TABLE 1. Annual mean values of surface temperature ($^{\circ}\text{C}$) and surface energy balance components (W m^{-2}) for 20-yr averages around the time of CO_2 doubling at year 70 in 1% yr^{-1} compound CO_2 increase experiments for the DOE coupled model and the CSM coupled model, for global averages, western Pacific area averages, and eastern Pacific area averages. The sign convention for absorbed shortwave is positive downward (i.e., positive sign means more energy enters the surface) and for the other components is positive upward (i.e., positive sign means more energy leaves the surface).

	Surface energy balance	
	$2 \times \text{CO}_2$ minus control	
	Coupled DOE	Coupled CSM
Global		
ΔT_s	+3.50	+1.43
Absorbed shortwave	+3.89	-0.79
Net infrared	-1.44	-2.57
Sensible	-0.63	-0.97
Latent	+3.03	+1.89
Western Pacific area (5°N - 5°S , 140° - 170°E)		
ΔSST	+2.27	+1.11
Absorbed shortwave	-1.17	-2.61
Net infrared	-0.14	-3.90
Sensible	+0.95	-0.48
Latent	-2.22	+3.80
Ocean heat convergence	-0.24	+2.03
Eastern Pacific area (5°N - 5°S , 120° - 90°W)		
ΔSST	+3.24	+1.07
Absorbed shortwave	+1.25	-3.06
Net infrared	-1.92	-4.29
Sensible	+0.95	-0.59
Latent	+6.77	+0.68
Ocean heat convergence	+4.55	-1.14

system in the west, and about 8 W m^{-2} more energy enters the system in the east). These changes in cloud forcing appear to be associated with dynamically coupled feedbacks between the atmosphere and ocean (as in El Niño), linked to the slackening SST gradient in the DOE model associated with decreased trade winds, and reduced upwelling in the east as evidenced by convergence of heat in the upper ocean of $+4.55 \text{ W m}^{-2}$ (Table 1). However, in the CSM the net cloud radiative forcing changes across the Pacific have the opposite sign compared to the DOE model, $+1.14 \text{ W m}^{-2}$ in the west, and -0.89 W m^{-2} in the east. The ocean dynamical response is also opposite in sign, with a divergence of heat in the east of -1.14 W m^{-2} and convergence in the west of $+2.03 \text{ W m}^{-2}$. Both the cloud forcing changes and the ocean dynamical response would contribute to the somewhat greater SST warming in the west compared to the east in the CSM, opposite to an El Niño-like response.

For the CSM there is a decrease of absorbed solar radiation at the surface in the west of -2.61 W m^{-2} (Table 1) in association with an increase in magnitude of cloud shortwave forcing of -1.55 W m^{-2} (Table 2). There are small changes of less than 1 W m^{-2} in sensible heat flux in the western Pacific for the CSM in Table 1, though there is an increase of downward IR that produces a decrease of net upward IR (-3.90 W m^{-2}) associated with an increase of cloud longwave forcing (shown in Table 2) of $+2.69 \text{ W m}^{-2}$. This was not evident in the western Pacific in the DOE model where the difference in net upward IR was less than 1 W m^{-2}

TABLE 2. Annual mean top-of-atmosphere values of cloud radiative forcing components (W m^{-2}), surface temperature ($^{\circ}\text{C}$), and changes in total cloud (%) from the various model experiments described in the text for global averages, western Pacific area averages, and eastern Pacific area averages. For cloud-forcing changes, the sign convention is positive downward (i.e., positive sign of a difference denotes more energy enters the system).

	$2 \times \text{CO}_2$ minus control					
	Coupled DOE	Coupled CSM	DOE slab	CCM3 slab diagnostic	CCM3 slab prognostic	CCM3 slab prognostic minus diagnostic
Global						
ΔT_s	+3.50	+1.43	+4.58	+2.08	+1.96	-0.08
$\Delta\text{Cloud shortwave}$	+4.73	-0.70	+4.76	-0.80	-1.06	-0.26
$\Delta\text{Cloud longwave}$	-0.87	-0.30	-0.30	-0.09	-0.08	-0.01
$\Delta\text{Cloud forcing}$	+3.86	-1.00	+4.46	-0.89	-1.14	-0.25
$\Delta\text{Cloud total}$	-4.5%	-0.3%	-5.6%	-0.3%	+0.6%	+0.9%
Western Pacific area (5°N - 5°S , 140° - 170°E)						
ΔSST	+2.27	+1.11	+2.99	+1.34	+1.34	0.0
$\Delta\text{Cloud shortwave}$	-0.40	-1.55	-1.03	-1.97	-2.82	-0.85
$\Delta\text{Cloud longwave}$	-5.07	+2.69	-10.08	-0.12	-0.06	+0.06
$\Delta\text{Cloud forcing}$	-5.47	+1.14	-11.11	-2.09	-2.88	-0.79
$\Delta\text{Cloud total} (\%)$	-3.6%	+1.9%	-8.0%	+1.2%	-0.3%	-1.5%
Eastern Pacific area (5°N - 5°S , 120° - 90°W)						
ΔSST	+3.23	+1.07	+3.61	+1.45	+1.76	+0.31
$\Delta\text{Cloud shortwave}$	+1.82	-1.51	-1.45	-3.43	+2.27	+5.70
$\Delta\text{Cloud longwave}$	+5.79	+0.62	+13.46	-0.17	+1.54	+1.71
$\Delta\text{Cloud forcing}$	+7.61	-0.89	+12.01	-3.60	+3.81	+7.41
$\Delta\text{Cloud total} (\%)$	+0.6%	+2.2%	+0.8%	+12.1%	+4.5%	-7.6%

(Table 1). However, in the CSM the increase of SST in the western Pacific area of 1.11°C contributes, along with an increase in surface winds, to an increase of latent heat flux from the surface of $+3.80\text{ W m}^{-2}$, while in the DOE model the latent heat flux actually decreases by -2.22 W m^{-2} , due to a decrease in surface winds (not shown). In the west in CSM there is a net heat convergence in the upper ocean of $+2.03\text{ W m}^{-2}$ that contributes to an increase of SST. This leaves the decrease of absorbed solar radiation of -2.61 W m^{-2} and net cloud forcing of $+1.14\text{ W m}^{-2}$ as contributors to the relatively lower SST increase due to increased CO_2 in the CSM compared to DOE. This can be compared to what occurred in the DOE model in the western equatorial Pacific where the net cloud forcing was -5.47 W m^{-2} , and there was a decrease of absorbed solar radiation at the surface of -1.17 W m^{-2} . But the decrease of latent heat flux in DOE noted above contributes to a larger SST increase compared to CSM where latent heat flux increased (a decrease of latent heat flux means less energy is removed from the surface).

In the eastern Pacific there are significant differences in the cloud responses resulting from increased CO_2 in the CSM compared to the DOE model. The similar SST increase in the east compared to the west in the CSM (1.07° vs 1.11°C) is associated with a comparable decrease of absorbed solar radiation in Table 1 as well (-3.06 vs -2.61 W m^{-2}). Recall that in the DOE model in Table 1, there was an increase of absorbed solar radiation at the surface in the east ($+1.25\text{ W m}^{-2}$) compared to the decrease of absorbed solar radiation noted above (-3.06 W m^{-2}). This is associated with a change in cloud radiative forcing due to increased CO_2 of $+7.61\text{ W m}^{-2}$ in the DOE model. Consistent with the similar differences in absorbed solar radiation at the surface in the CSM, the cloud shortwave forcing differences in east and west areas are -1.51 and -1.55 W m^{-2} , respectively. Therefore, in the CSM in the east there is a change of -0.89 W m^{-2} in net cloud forcing, while in the DOE model in the east there is a change of $+7.61\text{ W m}^{-2}$ in net cloud forcing (Table 2). Thus the biggest differences in cloud forcing and SST response between the two models occur in the eastern equatorial Pacific and are associated with an increase of ocean heat convergence of $+4.55\text{ W m}^{-2}$ in the DOE model compared to a decrease of -1.14 W m^{-2} in the CSM.

In a study using both a simple tropical Pacific coupled model and an ocean GCM with imposed SST dependent heat flux, when a uniform heating is applied across the Pacific to mimic what may occur with an increase in CO_2 , the cold tongue intensifies producing a La Niña-like response (Cane et al. 1997). However, as can be seen in Table 2, what starts out as a uniform positive radiative forcing from increasing CO_2 in the DOE model quickly becomes asymmetric across the Pacific due to contributions from the cloud radiative forcing response.

Some insight into the physical mechanisms causing these changes can be gained by looking at the changes

in the context of large-scale dynamical regimes (Bony et al. 1997). Using vertical velocity at 500 hPa as an index of large-scale vertical motion, in both CSM and DOE the western Pacific area is a large-scale rising-motion regime (values of ω of -19.87 and $-28.51\text{ hPa day}^{-1}$, respectively), while the eastern Pacific area in both represents large-scale descending motion (values of ω of $+18.23$ and $+19.27\text{ hPa day}^{-1}$, respectively). For the change with increasing CO_2 , relative changes of large-scale motion and SST, $\Delta\omega/\Delta\text{SST}$, for the western Pacific area for CSM and DOE are -3.12 and $-2.29\text{ hPa day}^{-1}\text{ K}^{-1}$, respectively, and for the eastern Pacific area -1.37 and $-2.81\text{ hPa day}^{-1}\text{ K}^{-1}$, respectively. These fall into the case-III category of Bony et al. (1997) denoting weak vertical motion changes associated with SST changes. Even with these weak changes in vertical motion, the El Niño-like response can be seen in the DOE model with somewhat greater increase of rising motion in the east compared to the west (-2.81 vs $-2.29\text{ hPa day}^{-1}\text{ K}^{-1}$), while the relative change in vertical motion is greater in the west compared to the east in CSM (-3.12 vs $-1.37\text{ hPa day}^{-1}\text{ K}^{-1}$). Thus the large-scale control over cloud changes with global warming are weak, and, as noted by Bony et al. (1997), the cloud radiative feedbacks are more related to the thermodynamical effect of SST changes on cloud parameters.

The "sensitivity index," \bar{I}_x , of Bony et al. (1997) is computed for the cloud-forcing changes noted in Table 2 for the eastern and western Pacific areas (\bar{I}_x computed for case-III situations as noted above), and is defined as

$$\bar{I}_x = \frac{\Delta x \Delta \text{SST}}{\Delta \text{SST}^2},$$

where Δx is the difference of a cloud radiative forcing quantity for increased CO_2 minus control, and ΔSST is the change in SST.

The change in cloud shortwave forcing, \bar{I}_{CSW} , for the western Pacific area for CSM and DOE is -1.39 and $-0.18\text{ W m}^{-2}\text{ K}^{-1}$, respectively. For CSM this is related to an increase of cloud ($+1.9\%$ in Table 2) as could be expected over a warm ocean region (27.9°C for CSM) noted by Bony et al. (1997). Though total cloud decreases in DOE (-3.6%), the increase of convective clouds with somewhat higher albedo contribute to the small negative value of \bar{I}_{CSW} . However, there is an opposite sign change of \bar{I}_{CLW} of $+2.42$ versus $-2.23\text{ W m}^{-2}\text{ K}^{-1}$ for CSM and DOE, respectively, in the west. As noted by Bony et al. (1997), for a warm ocean regime an increase of cloud longwave forcing generally is associated with deeper convection and colder cloud tops. For the CSM, this is indicated by an increase of convective mass flux of $+19.7\%$ at $\sigma = 0.288$ in the upper troposphere in the western Pacific area. For DOE, as noted above there is a decrease in total cloud and less very deep convection (cumulus cloud frequency count decreases -57% at $\sigma = 0.189$ in the upper troposphere).

Thus, even though the changes in vertical motion are considered to be weak, there still appears to be some influence of large scale dynamical changes. As noted by Bony et al. (1997), for very warm SSTs (above 29.5°C, and SST for the western Pacific area for DOE is 29.8°C), an increase of SST should be associated with a decrease of \bar{I}_{CLW} which in fact was noted in the DOE model. This occurs because strong rising motion is still prevalent, but there are some weak subsiding motions (as noted above $\Delta\omega/\Delta\text{SST}$ had larger amplitude in the eastern than western Pacific associated with the El Niño-like response in DOE) that affect the overall amount of deep convection in the west in the DOE model, thus reducing the cloud longwave forcing. For \bar{I}_{NET} , the cloud longwave forcing change dominates for CSM and DOE in the west producing values of +1.03 and $-2.41 \text{ W m}^{-2} \text{ K}^{-1}$, respectively.

For the eastern Pacific area, \bar{I}_{CSW} is $-1.41 \text{ W m}^{-2} \text{ K}^{-1}$ for CSM, and $+0.56 \text{ W m}^{-2} \text{ K}^{-1}$ for DOE. The change for CSM could be expected from the analysis of Bony et al. (1997) due to the increase in clouds in the eastern area (+2.2%). The value of $+0.56 \text{ W m}^{-2} \text{ K}^{-1}$ for DOE is associated with an increase of convective cloud with smaller cloud fraction thus reducing albedo by -4.7% , even though there is a slight increase in total cloud of $+0.6\%$ in Table 2. Bony et al. (1997) note that over a cold ocean region such as the eastern Pacific (25.0°C for CSM), small changes in \bar{I}_{CLW} should be expected with warming of SSTs (only $+0.58 \text{ W m}^{-2} \text{ K}^{-1}$ for CSM). However, for DOE that value for cloud longwave forcing is $+1.79 \text{ W m}^{-2} \text{ K}^{-1}$. In this case the warmer base state in the eastern Pacific in the DOE model (26.4°C) affects the cloud longwave response. Thus the DOE behavior in the eastern Pacific is more like the warm ocean regime of Bony et al. (1997), where an increase of \bar{I}_{CLW} is accompanied by deeper convection and colder cloud tops (cumulus cloud frequency increases $+103\%$ at $\sigma = 0.189$ in the upper troposphere in the east in DOE). For CSM, the change in \bar{I}_{NET} of $-0.83 \text{ W m}^{-2} \text{ K}^{-1}$ is dominated by the change in \bar{I}_{CSW} , while both \bar{I}_{CSW} and \bar{I}_{CLW} with positive signs add to produce an \bar{I}_{NET} for DOE of $+2.36 \text{ W m}^{-2} \text{ K}^{-1}$. Therefore, the base-state SSTs in the control runs contribute to the nature of the cloud forcing response with increased CO_2 .

In Table 2, cloud-forcing quantities are shown for the atmospheric models coupled to nondynamic slab oceans. As noted above, this type of experiment with increasing CO_2 is instructive to remove amplifying effects of ocean dynamics. Therefore, these results should more accurately portray small initial asymmetries that could occur because of a nearly uniform warming of SSTs across the Pacific with increasing CO_2 , in addition to examining parameter-dependent aspects of the cloud radiative response. There are several tenths of a degree difference in the SST response between western and eastern Pacific in the slab model versions, with the largest SST asymmetries in the CCM3 with prognostic cloud

liquid water ($+1.34^\circ\text{C}$ in the west, $+1.76^\circ\text{C}$ in the east) and in the DOE model ($+2.99^\circ\text{C}$ in the west, $+3.61^\circ\text{C}$ in the east). The column at right in Table 2 gives the differences of the response between the CCM3 versions to portray how differences in cloud liquid water parameterization affect the cloud radiative forcing response (prognostic cloud liquid water minus diagnostic cloud liquid water; SSTs are similar in the control integrations). The differences are mostly less than 1 W m^{-2} except for a large difference of $+5.70 \text{ W m}^{-2}$ for cloud shortwave forcing in the eastern Pacific that is associated with a net cloud forcing with a comparably large positive value ($+7.41 \text{ W m}^{-2}$). These large positive differences are produced by a change in sign in the cloud shortwave forcing in the eastern Pacific between the diagnostic (-3.60 W m^{-2}) and prognostic ($+3.81 \text{ W m}^{-2}$) schemes, associated with a greater increase ($+12.1\%$) of total cloud in the diagnostic compared to $+4.5\%$ in the prognostic. Though changes in total cloud do not translate directly to comparable changes in cloud shortwave forcing (note larger positive difference in cloud longwave forcing in CCM3 prognostic), the model with the larger increase of cloud amount (CCM3 diagnostic) has the greater negative difference in cloud shortwave forcing. Thus, the more physically realistic prognostic scheme produces an asymmetric cloud radiative forcing with increased CO_2 compared to the diagnostic scheme.

Additionally, it has been suggested that a relaxing of the SST gradient across the equatorial Pacific with increasing CO_2 (whereby the SSTs in the eastern Pacific warm more than in the west, the El Niño-like response) could be associated with an east–west differential in evaporative damping that could regulate the relative warming rates with increasing CO_2 (Knutson and Manabe 1995). To investigate this mechanism in the models under consideration here, the west minus east SST change in the increased CO_2 minus control experiments shown in Table 1 are -0.97° and $+0.04^\circ\text{C}$ for the coupled DOE and CSM models, respectively. The change in latent heat flux for west minus east for the DOE model is -8.99 W m^{-2} . The sign indicates that this latent heat flux differential should act to intensify the cold tongue (in Table 1, $+6.77 \text{ W m}^{-2}$ latent heat flux change in the east, positive sign denoting energy removed from the surface, and -2.22 W m^{-2} change in the west). However, the DOE model SST response is a relative warming of the cold tongue region. For the CSM this west minus east change in latent heat flux is $+3.12 \text{ W m}^{-2}$, with the sign indicating that the latent heat flux change should act to slacken the SST gradient (in Table 1, $+3.80 \text{ W m}^{-2}$ removed from the surface in the west due to latent heat flux change compared to only $+0.68 \text{ W m}^{-2}$ in the east). However, the CSM produces little change in the SST gradient. Meanwhile, the change of cloud radiative forcing, west minus east, is -13.08 W m^{-2} in the DOE model (the negative sign indicative of a contribution to slackening the west–east SST gradient) and only $+2.03$

W m^{-2} in the CSM. Thus in the DOE model with the large El Niño-like response, the west minus east change in cloud forcing is about +45% greater than the contribution from changes in latent heat flux but nearly comparable in the CSM with no El Niño-like response.

A more instructive example of the contributions from latent heat flux changes in the absence of ocean dynamical responses can be obtained from the slab ocean simulations. For the CCM3 case with diagnostic cloud liquid water (CCM3 diagnostic), the SST change, west minus east, is -0.11°C , while the value from CCM3 with prognostic cloud liquid water (CCM3 prognostic) is -0.42°C (Table 2). The west minus east difference for cloud forcing changes for $2 \times \text{CO}_2$ minus control is $+1.51 \text{ W m}^{-2}$ for CCM3 diagnostic (acting to intensify the cold tongue), and -6.69 W m^{-2} for CCM3 prognostic (acting to relax the SST gradient). Meanwhile, the change in latent heat flux, west minus east, is $+1.01 \text{ W m}^{-2}$ for CCM3 diagnostic (positive sign indicates a contribution to slacken the SST gradient), while it is -2.74 W m^{-2} for CCM3 prognostic (acting to intensify the SST gradient; these latent heat flux changes not shown in Table 2). Thus, the changes from cloud radiative forcing, compared to latent heat flux changes, are larger by more than a factor of two in the CCM3 prognostic, while more nearly the same for the CCM3 diagnostic. Thus for these slab ocean models, the east–west change in cloud radiative forcing for an increase in CO_2 with the prognostic cloud liquid water scheme is the dominant contributor to an asymmetric radiative forcing across the Pacific.

5. Model evaluation from Atmospheric Model Intercomparison Project (AMIP) integrations

The difference in tropical response in the two coupled models, traced in part to cloud forcing changes, raises questions as to which is more likely to occur in the real climate system. One way of assessing the realism of cloud forcing changes in the models is to compare the responses of their atmospheric components to the change in SST between the 1986/87 El Niño event and the 1988/89 La Niña event with observations using the AMIP integration results (Gates 1992).

The DOE model has a simple cloud albedo feedback scheme that produces changes only when SSTs exceed 29.8°C (Washington and Meehl 1993). This threshold was chosen because the slab ocean and fully coupled versions of the DOE model have systematically warmer-than-observed SSTs (by about 1° – 2°C) in the control simulations (Washington and Meehl 1993). Cloud albedo changes occur almost exclusively in the warmest regions of the western Pacific and essentially not at all in the cold tongue region in the east.

The version of the CCM3 in the CSM used here has a parameterized diagnostic cloud liquid water path response, whereby changes in scale height cause a shift of the specified liquid water path profile in the middle

and upper troposphere (Hack 1998). This parameterization is likely to capture cloud processes more realistically in a deep convective regime such as the western Pacific warm pool region, since water vapor there would more likely be mixed throughout the depth of the troposphere and so affect cloud liquid water path. Though tested and verified in relation to observations in an earlier version of the atmospheric model (CCM2) with a different convective scheme (Hack 1998), this scheme appears to not work as well in the eastern Pacific with the revised convective scheme in CCM3 (Kiehl et al. 1998). An improved version of the CCM3 with a prognostic cloud liquid water scheme (Rasch and Kristjansson 1998) has been designed and tested in the CCM3 to simulate the mean state more realistically.

Table 3 shows changes in SST and cloud forcing for the difference of a warm DJF (1986/87) minus a cold DJF (1988/89) for top-of-atmosphere quantities from integrations with the DOE atmospheric model, the CCM3 with diagnostic cloud liquid water (as used in the CSM), and the CCM3 with prognostic cloud liquid water. Observations from the Earth Radiation Budget Experiment (ERBE) are also listed at the right in Table 3. Additional ensemble members (two are averaged for CCM3 diagnostic) show similar cloud radiative forcing changes.

The observed SST change for El Niño minus La Niña for these specified SST integrations is $+0.08^{\circ}\text{C}$ in the western Pacific and $+1.69^{\circ}\text{C}$ in the east (Table 3). Therefore, the atmospheric models are being driven by a large zonally asymmetric surface temperature anomaly. The responses in the two CCM3 versions are similar. Both have increased albedo by over 10% and increases of total clouds by around 5% in the west, with decreases in albedo of over 5% and small increases in total cloud of less than 5% in the east. The signs of changes of cloud shortwave and cloud longwave forcings are also similar in the two CCM3 versions, with the only notable difference appearing in the net cloud radiative forcing in the western area where there is an increase of $+4.57 \text{ W m}^{-2}$ in CCM3 diagnostic and a decrease of -2.03 W m^{-2} in CCM3 prognostic. The signs of the various cloud forcing changes agree with observations (Table 3), except for the observed decrease in net cloud forcing of -1.8 W m^{-2} in the west. This agrees with the net cloud radiative forcing change in CCM3 prognostic (-2.03 W m^{-2}) but not with CCM3 diagnostic ($+4.57 \text{ W m}^{-2}$).

Net cloud forcing is larger (positive) in the east compared to the west in both CCM3 versions, indicating an asymmetric cloud radiative response has resulted from a large asymmetric SST forcing. Both CCM3 versions also experience comparable increases of cloud liquid water in the west (greater than 30%) and decreases in the east (from about -18% to -25%). As noted above, in the DOE model the cloud albedo response only operates when SST exceeds 29.8°C (Washington and Meehl 1993). For the AMIP experiments, the warmest

TABLE 3. Changes in SST ($^{\circ}\text{C}$), cloud radiative forcing components (W m^{-2}), albedo (%), cloud water (%), and total cloud (%) for the difference of a warm DJF (1986/87) minus a cold DJF (1988/89) for top-of-atmosphere quantities from integrations with the DOE atmospheric model, the CCM3 with diagnostic cloud liquid water (as used in the CSM), and the CCM3 with prognostic cloud liquid water. Observations from ERBE are listed at right. For cloud forcing changes, the sign convention is positive downward (i.e., positive sign of a difference denotes more energy enters the system).

AMIP, top of atmosphere				
1986/87 minus 1988/89 (warm minus cold)				
	DOE	CCM3 Diagnostic (average of 2)	CCM3 Prognostic	Observed
Global ΔT_s ($^{\circ}\text{C}$)	+0.17	-0.04	+0.23	+0.06
Western Pacific area (5°N - 5°S , 140° - 170°E)				
ΔSST ($^{\circ}\text{C}$)	+0.08	+0.08	+0.08	+0.08
Top of atmosphere (W m^{-2}):				
$\Delta\text{Cloud shortwave}$	+7.25	-10.66	-12.82	-27.63
$\Delta\text{Cloud longwave}$	+5.15	+15.23	+10.79	+25.92
$\Delta\text{Cloud forcing}$	+12.40	+4.57	-2.03	-1.71
ΔAlbedo (%)	-6.5%	+10.7%	+12.5%	+4.2%
$\Delta\text{Cloud total}$ (%)	+2.2%	+5.8%	+4.6%	—
$\Delta\text{Liquid water}$ (%)	—	+39.3%	+34.0%	—
Eastern Pacific area (5°N - 5°S 120° - 90°W)				
ΔSST ($^{\circ}\text{C}$)	+1.69	+1.69	+1.69	+1.69
Top of atmosphere (W m^{-2}):				
$\Delta\text{Cloud shortwave}$	+2.23	+13.51	+7.68	+1.28
$\Delta\text{Cloud longwave}$	+13.04	+5.18	+4.72	+2.80
$\Delta\text{Cloud forcing}$	+15.27	+18.69	+12.40	+4.08
ΔAlbedo (%)	-0.2%	-11.1%	-6.1%	+1.7%
$\Delta\text{Cloud total}$ (%)	+8.7%	+1.4%	+4.5%	—
$\Delta\text{Liquid water}$ (%)	—	-25.4%	-18.3%	—

area-averaged SST in 1988/89 in the west is only around 29°C . Since SSTs are usually less in the west and always less in the east (not only in the mean but also during the 1986/87 and 1988/89 events) the cloud albedo response would rarely be activated in the DOE model. This is reflected in part by a net cloud forcing in the west of $+12.40 \text{ W m}^{-2}$ and a decrease of albedo of -6.5% . However, changes in cloud type (e.g., MW96) produce proportionately greater net cloud forcing in the east ($+15.27 \text{ W m}^{-2}$) to provide relatively more energy input to the system from cloud forcing in the east compared to the west in 1986/87 compared to 1988/89.

None of the models' cloud-forcing response verifies particularly well with the observations. The two CCM3 versions show the greatest difference in response in the west with a net positive cloud forcing of $+4.57 \text{ W m}^{-2}$ with CCM3 diagnostic and -2.03 W m^{-2} with CCM3 prognostic, with the latter agreeing better with the observed difference of -1.71 W m^{-2} . Of greatest interest is comparing the cloud forcing response in the east between the slab ocean versions of CCM3 (Table 2) and the AMIP versions (Table 3). When given a strong SST forcing from below as in the AMIP simulations, both CCM3 versions produce positive cloud forcing changes in the east ($+18.69 \text{ W m}^{-2}$ for CCM3 diagnostic and $+12.40 \text{ W m}^{-2}$ for CCM3 prognostic). Though both forcing changes are larger than the observed change by greater than a factor of 3, they agree with the obser-

variations in sign. However, the results change markedly when the SSTs are allowed to interact and respond to the atmosphere, as in the slab ocean integrations for $2 \times \text{CO}_2$. CCM3 diagnostic shows a change in the east of -3.60 W m^{-2} in response to warming (Table 2) compared to $+18.69 \text{ W m}^{-2}$ in the AMIP case (Table 3). For $2 \times \text{CO}_2$, CCM3 prognostic has a reduced-amplitude change in the east but maintains the same sign as in the AMIP case, from $+12.40 \text{ W m}^{-2}$ (Table 3) to $+3.81 \text{ W m}^{-2}$ (Table 2). This result agrees better with the observed values, but it corresponds to a much larger SST change than in the observations.

Although there are clear limitations in using AMIP runs for model evaluation (since interacting quantities can affect the sign of the response), the above results suggest that CCM3 prognostic is probably capturing the observed cloud responses better than CCM3 diagnostic, and that both models are performing better than the DOE model. However, the high albedo-change threshold used in the DOE model makes it difficult a priori for this model to perform well in the AMIP case. In terms of assessing overall model credibility, therefore, the AMIP evaluation is somewhat inconclusive.

6. Response at high northern latitudes

A second significant regional response in climate change experiments that contributes to global warming

involves changes of sea ice. Several techniques have been proposed to estimate the contribution of ice albedo feedback to the global response in climate models (e.g., Dickinson et al. 1987; Schlesinger 1989). Here we apply a variant of the technique used in Dickinson et al. (1987). As noted by U. Cubasch et al. (1999, unpublished manuscript), in a coupled model transient simulation there is a nonequilibrium adjustment to the net heating perturbation. Additionally, as noted by Dickinson et al. (1987) and others, such feedbacks cannot be expected to add in a simple fashion. For our purposes here we will compute the most simple estimate for a contribution to global warming due to changes in ice and snow to estimate the relative size of such a contribution at the time of CO₂ doubling, with the additional caveat that this relative contribution only applies at that time in the experiment. Presumably the final equilibrium contribution would be somewhat different as noted by U. Cubasch et al. (1999, unpublished manuscript). The global average surface temperature change ΔT in a CO₂ increase experiment can be interpreted in terms of a zero-dimensional steady-state climate model written as

$$\lambda \Delta T = \Delta Q,$$

where ΔQ is the external heating perturbation from doubled CO₂ and λ is the sum of various feedbacks. For a ΔQ from the CSM of 3.54 W m⁻² and ΔT of 1.43°C at the time of CO₂ doubling (Table 1), λ is 2.48 W m⁻² K⁻¹. Assuming the globally averaged change in net clear-sky absorbed solar radiation at the surface (+0.86 W m⁻² for the CSM) is mostly due to changes in ice and snow, following the technique in Dickinson et al. (1987) the contribution to λ is 0.60 W m⁻² K⁻¹ (0.86 W m⁻² divided by 1.43°C). Thus following the assumptions above, the value of λ without the contribution from changes in ice and snow is 3.08 W m⁻² K⁻¹ and produces a global warming of 1.15°C if the effects of ice/snow changes are removed. This is a reduction of global warming of 0.28°C, or 20%. For the DOE model, the global warming is 3.50°C and λ is 1.01 W m⁻² K⁻¹. The change in net clear-sky absorbed solar radiation at the surface is +2.07 W m⁻². If snow/ice changes are removed, λ increases to 1.60 W m⁻² K⁻¹, and the resulting global warming is 2.21°C, a reduction of 37%. Thus the snow-ice response in the DOE model is stronger than in the CSM and contributes more to global warming with increasing CO₂. Though this is a combined contribution of ice and snow changes, it has been shown that most of the positive feedback is a result of sea-ice retreat and associated ocean heat storage changes at the ice margins (Robock 1983; Washington and Meehl 1984).

At least two factors contribute to this reduced high-latitude response in the CSM in comparison with the DOE model. First, the CSM ocean includes the Gent-McWilliams (GM) isopycnal mixing scheme (Gent et al. 1998). It has been shown that the circumpolar southern ocean warms less in an idealized global warming

experiment with this scheme included in an ocean model (Power and Hirst 1997). Though difficult to quantify in the present context, the results of Power and Hirst (1997) indicate that, at middle and high southern latitudes, there would be a smaller sea-ice contribution to warming in the CSM with GM mixing in comparison with the DOE model with conventional horizontal-diffusion mixing.

Second, the DOE model communicates atmospheric fluxes to the ocean-ice surface using an area-averaged albedo threshold (i.e., if the threshold is exceeded, a grid box can appear to be ice-free to the atmosphere and in fact there is still some ice left in the grid box), and the CSM uses an area-weighted ice fraction. It has been shown that the former is more sensitive than a scheme that requires ice in the entire grid box to melt before the albedo changes entirely to the lower ocean albedo value (Meehl and Washington 1990). Thus, the DOE model with the ice threshold technique would be expected to have greater sea-ice response and larger amplitude warming compared to the CSM with surface fluxes area-weighted by ice fraction.

Though there are contributions to sea-ice response in both hemispheres, the Arctic tends to have a proportionately greater contribution to sea-ice response in transient simulations because of ocean thermal inertia in the Southern Ocean (Kattenberg et al. 1996; Fig. 4 for the CSM). Thus, the Arctic region was highlighted in the study of WM96 and will be the focus of the present discussion for the CSM to illustrate sea-ice response.

It was noted by WM96 that as CO₂-induced warming and sea-ice melting occurred at high northern latitudes in the DOE coupled model, there were increases in low clouds at high latitudes. In contrast, in most areas clouds decreased because of warmer temperatures and lower relative humidity. The albedo increases from these clouds were not sufficient to offset the decreases in albedo from formerly ice-covered grid points, however, so planetary albedo at high latitudes decreased. Additionally, warmer water from the ice-free North Atlantic in the CO₂ experiment was transported northward toward the Arctic, also contributing to melting the sea ice. WM96 concluded that a combination of these factors contributed to an unusually strong sea-ice response leading to enhanced global warming in the DOE model.

While there are long-term trends in the control run and decadal timescale changes in total sea ice of both signs as the climate warms with increasing CO₂ in the CSM, the overall trend is toward decreasing ice coverage with the biggest decreases in the Arctic (Fig. 4). Figure 5 shows sea-ice thickness distributions for maximum (March) and minimum (September) ice extents in the CSM for control and increased CO₂. These can be compared with Figs. 3a-d in WM96. Consistent with the lower climate response of the CSM, the changes in total sea ice area are smaller than in the DOE model.

Greatest decreases in ice area of -23% occur in September in the CSM (in comparison with -15% in

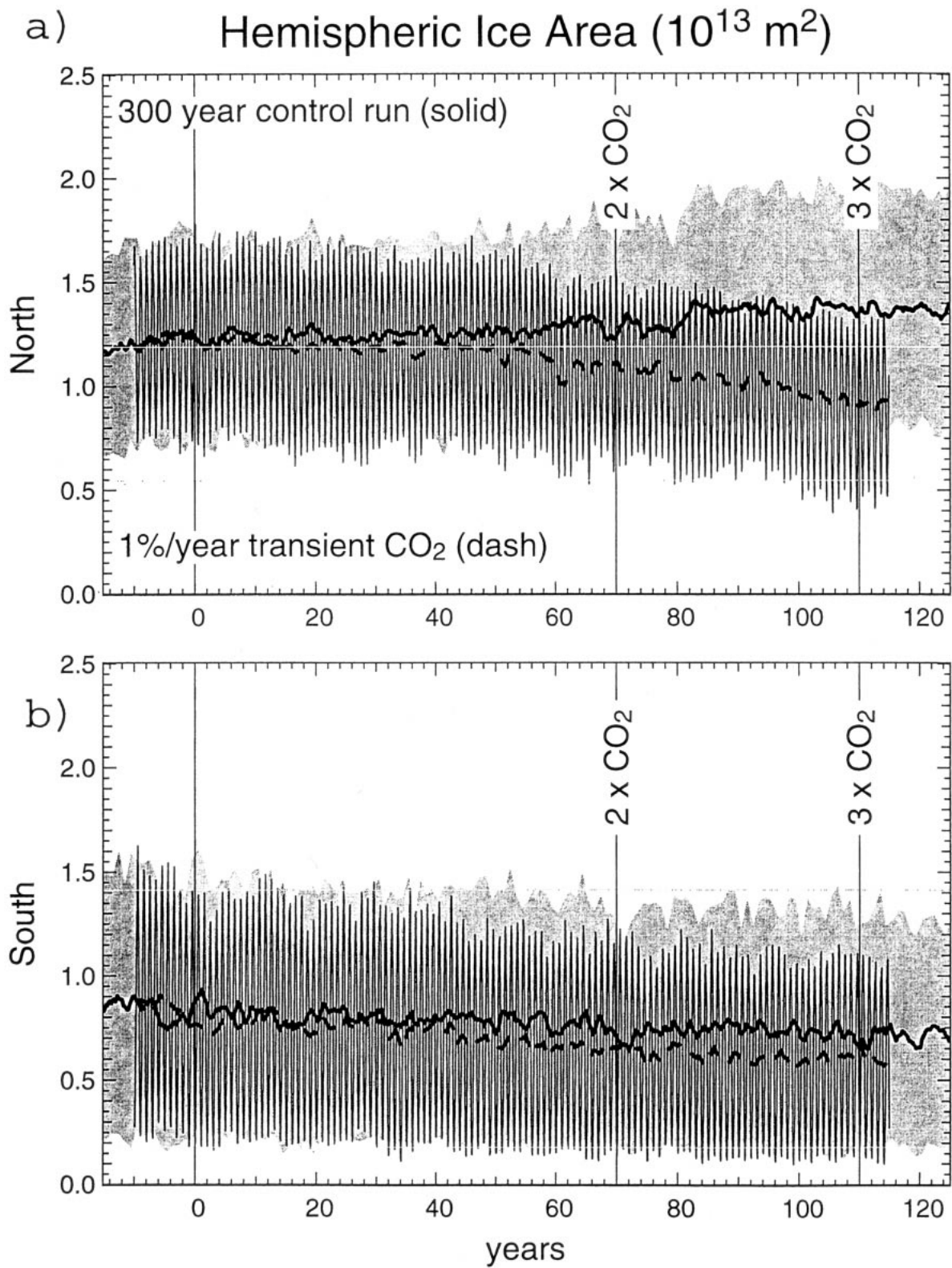


FIG. 4. Time series of hemispheric sea-ice area from the control run (solid black line is smoothed value, shaded gray area is envelope of monthly values), and from the 1% transient CO_2 increase run from the NCAR CSM (dashed line is smoothed value, thin black line is monthly mean values) for (a) Northern Hemisphere and (b) Southern Hemisphere. Times when CO_2 doubles and triples are indicated. The doubled CO_2 time period is discussed in the current paper.

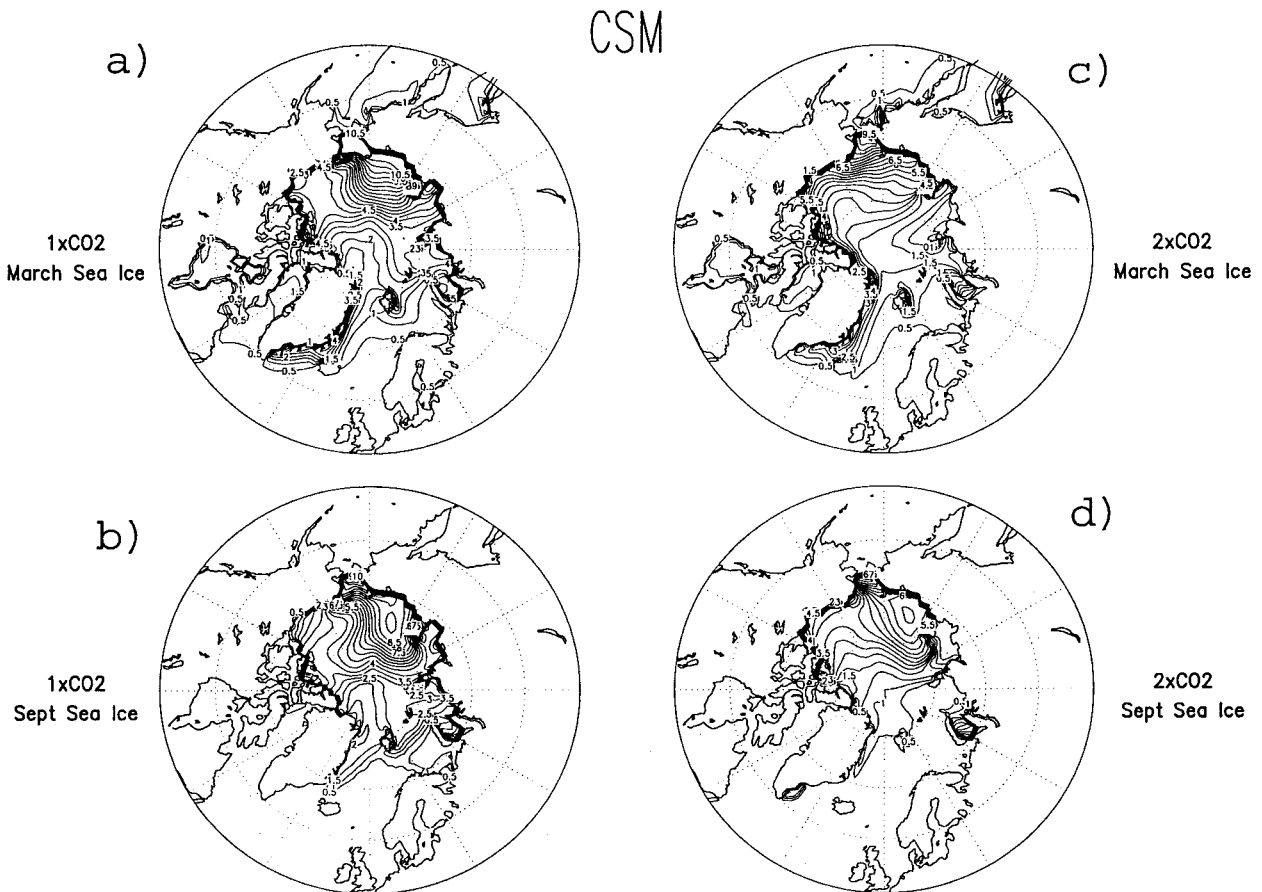


FIG. 5. (a) Mean sea-ice thickness (m) for 20-yr average (years 60–79) for Mar from the control integration of the NCAR CSM; (b) same as (a) except for Sep; (c) same as (a) except for the transient CO_2 increase experiment at time of CO_2 doubling; and (d) same as (b) except for the transient CO_2 increase experiment at time of CO_2 doubling.

March). Relative ice retreat in September, the low-ice part of the year, is important for increased absorbed solar radiation and less subsequent ice formation in winter. In these simulations, the Arctic remains ice-covered throughout the year even with increased CO_2 (Figs. 5c,d). These ice area changes are associated with atmospheric changes that may ameliorate or amplify the ice albedo changes. For example there is a decrease in low clouds over the ice-covered Arctic in March (Fig. 6a) due to mostly decreased relative humidity in the warmer air over the ice. In March, ice thickness decreases by about 30% (Fig. 4).

Latitudes where ice in the CSM has melted in the CO_2 case (near 60° – 70°N) experience an increase in low cloud in September (Fig. 6b) as is also seen in the DOE model. However, there is greater sea-ice coverage in the Arctic in the CSM (and more than observed; Weatherly et al. 1998) in comparison with the DOE model in the control case (40% more in September, and 47% more in March). This is particularly true in the Greenland–Iceland–Norwegian (GIN) Sea region, while the DOE model has less than observed (WM96). Some earlier modeling studies suggest that a model with greater ice

coverage and a colder control run should have larger ice albedo feedback and greater sensitivity (e.g., Spelman and Manabe 1984). However, later studies demonstrated how other factors such as the nature of the sea-ice formulation itself could complicate such a seemingly simple relationship (e.g., Meehl and Washington 1990). Here, changes in ocean dynamics and heat transport are also shown to play a significant role in the model responses involving sea ice.

As noted above, the biggest ice area changes in the CSM occur in September. Thus, we focus on that time of year in the following discussion. As the climate warms in the model from the increases of CO_2 , the ice-free GIN Sea surface also warms ($+2.53^\circ\text{C}$ in DOE and $+2.43^\circ\text{C}$ in CSM in September). As the ice melts, low clouds around 60° – 70°N increase in that region in September in the CSM (Fig. 6b) and in the DOE model (WM96, their Fig. 3f). This leads to an increase in albedo at the latitudes that were ice-free in the control run. Over the GIN Sea region in total, however, there is a net increase in absorbed solar radiation in the CSM of $+1.0 \text{ W m}^{-2}$ (ocean points in the area 60° – 80°N , 30°W – 30°E) mainly arising from areas that were for-

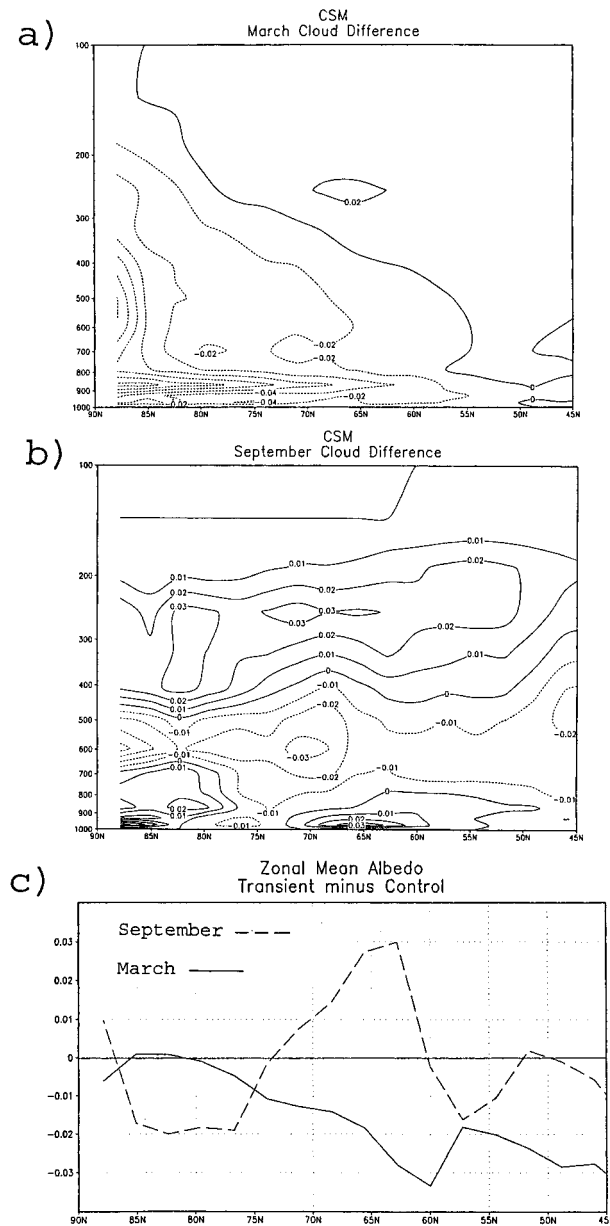


FIG. 6. (a) Zonally averaged Mar cloud differences, transient CO_2 increase (at time of CO_2 doubling) minus control, north of 45°N for 20-yr averages, years 60–79; solid lines indicate cloud increases in the transient CO_2 experiment; typical zonal mean low-cloud amounts in the control case in Mar near 65°N are around 0.70, and near 85°N are around 0.95; (b) same as (a) except for Sep; typical zonal mean low-cloud amounts in the control case in Sep are about 0.55, and near 85°N are roughly 0.85; (c) zonal mean planetary albedo difference for transient CO_2 increase minus control, north of 45°N for 20-yr averages, years 60–79, for Mar (solid) and Sep (dashed).

merly ice-covered from about 73° to 80°N (Figs. 5b and 6c). In contrast, in the DOE model, where there was little ice in the GIN Sea in the control run in September (WM96, their Fig. 3b) there is a net increase in albedo and a decrease in absorbed solar radiation (-3.21 W m^{-2}).

From these changes in absorbed solar radiation alone, one would expect greater sea-ice response in this region in the CSM in comparison with the DOE model, because there would be more energy available to melt ice in the former from the increase in absorbed solar radiation. However, as noted previously, the converse is true. This is because ocean dynamics and poleward heat transport are also involved. There is a greater decrease of the maximum of meridional overturning near 40°N in the DOE model [peak values decrease 41% from 41 to 24 Sverdrups $\equiv 10^6 \text{ m}^3 \text{ s}^{-1}$ (Sv)] in comparison with CSM (peak values decrease 3% from 33 to 32 Sv). However in Fig. 7 the overturning maximum in the GIN Sea (north of 65°N) decreases by 46% in the CSM (from about 6.5 to 3.5 Sv) in comparison with a smaller decrease of 20% in the DOE model (peak value decreases from about 2.5 to roughly 2 Sv). These changes are associated with decreases in upper-ocean density in the two models.

As noted previously, both models have comparable warming in the upper-ocean layers due to increased CO_2 . Both models, therefore, should show comparable increases in poleward ocean heat transport as this greater heat content is transported north, in the absence of mass transport rate changes. The relative overturning rate changes, however, imply that the models have different heat transport changes: the model with less weakening of the overturning should have greater relative increase in poleward ocean mass and, hence, heat transport to contribute to melting ice. Indeed this is the case. Both the CSM and DOE models have similar values of ocean heat transport near 60°N in the GIN Sea in their control integrations (0.36 Pw in CSM, 0.34 Pw in DOE, not shown). But associated with relatively stronger meridional overturning in the GIN Sea in the increased CO_2 experiment in the DOE model in comparison with the CSM (Fig. 7), the increase of poleward heat transport near 60°N is greater (+118% in the DOE model, +13% in CSM). These heat transport changes are sufficient to more than offset the influence of changes in absorbed solar energy, resulting in greater decreases of ice area with increased CO_2 in the DOE model in comparison with CSM. This, in turn, leads to greater warming over the Arctic in the DOE model.

7. Conclusions

To help to understand the global response to increasing CO_2 in the NCAR CSM, two regional physical processes are identified as being important to the magnitude of global warming: the “El Niño-like” response in the tropical Pacific and sea-ice response at high latitudes. These processes are compared in the NCAR CSM and the NCAR DOE coupled model. Global warming due to increased CO_2 is relatively low in the CSM as compared with the DOE model and other global coupled models.

The El Niño-like response to increased CO_2 has been

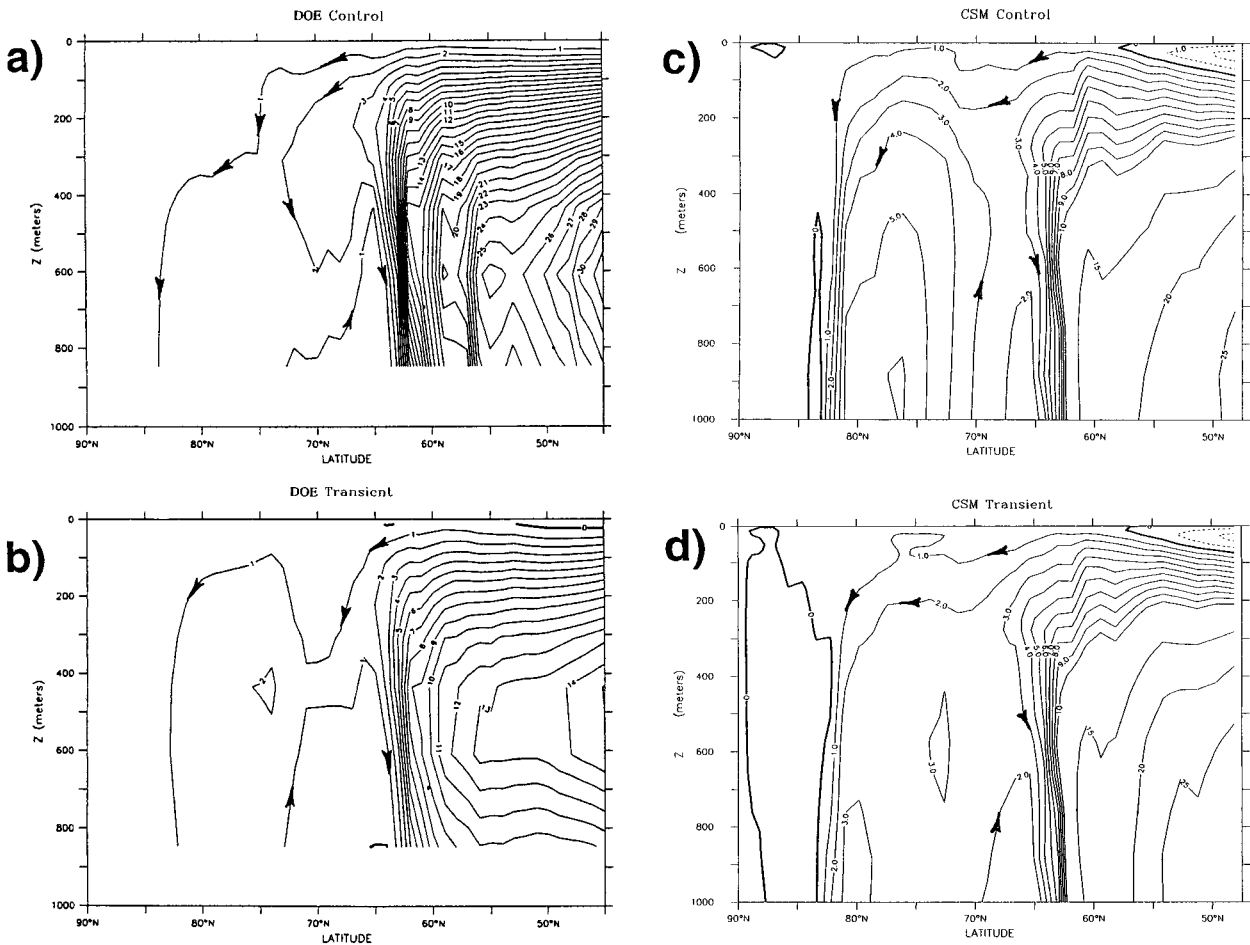


FIG. 7. (a) High-latitude Atlantic contribution (roughly north of 45°N) to annual zonal average ocean meridional volume transport (Sv), upper 1000 m, years 65–74, for the DOE model control integration; (b) same as (a) except for increased CO_2 experiment, years 65–74, near the time of CO_2 doubling (after Washington and Meehl 1996); (c) same as (a) except for CSM control; (d) same as (b) except for CSM near the time of CO_2 doubling.

characterized in previous studies by larger warming in the eastern Pacific in comparison with the west (as in the DOE model, i.e., a slackening of the west–east SST gradient). The sign of the global cloud feedback is positive in DOE and negative in CSM, and we hypothesize that cloud response (and, hence, the details of model cloud parameterizations) is a significant factor determining whether an El Niño–like response occurs. Similar cloud responses operate in the western equatorial Pacific in the DOE model and the CSM with negative net cloud forcing differences. In the eastern Pacific, however, the DOE model produces a large positive cloud radiative forcing difference relative to the west, and the CSM has a negative cloud radiative forcing difference. Thus, there is an asymmetric cloud radiative forcing response in the DOE model and not in the CSM, and little El Niño–like response to increased CO_2 in the CSM as compared with the DOE model.

Analyses of slab ocean versions of the CSM and DOE models are performed to remove the amplifying effects

of ocean dynamics and to study possible parameterization-dependent aspects of the response of the coupled models. A version of the CCM3 that includes prognostic cloud liquid water shows a change in sign (from negative to positive) of the net cloud forcing in the eastern equatorial Pacific (more similar to the DOE model) in comparison with the CCM3 version with diagnostic cloud liquid water used in the CSM.

In an attempt to determine which of the models' cloud parameterization schemes is more realistic, we use AMIP (prescribed SST) results to evaluate the different models. All three models (DOE, CCM3 diagnostic, and CCM3 prognostic) performed poorly relative to observations in terms of cloud radiative forcing response, although CCM3 prognostic was slightly superior to the other models. Specific details of the DOE cloud scheme, however, preclude a realistic response in the AMIP cases. Senior (1999) points out that future GCM simulations should be evaluated with different diagnostics such as absorption and extinction coefficients of clouds, and,

in particular, they should be compared directly with observable quantities such as variation of cloud optical thickness with temperature and the variation of cloud water path with droplet size. It is not possible at present, therefore, to judge which model is most realistic in the CO₂-increase case, so determining the likelihood of a future El Niño-like response requires further research. Additionally, Bony et al. (1997) suggest that the initial state could be important in determining the cloud feedbacks in the Pacific.

The effect of this response aspect on global warming also remains somewhat equivocal. Observational evidence (Jones 1988) shows that warm events in the Pacific have a distinct global warming signature, so it is likely that models with an El Niño-like response will have greater global warming. Indeed in a slab ocean version of the DOE model with a prescribed El Niño-like response, global warming was increased by 5%. However, the lower monsoon enhancement in the DOE model, which has already been linked to the model's El Niño-like response, could offset the direct warming influence if it were associated with a global-scale reduction in water vapor feedback. Further diagnostic studies of temperature, moisture, and cloud teleconnections in a greater number of models are required to resolve this issue.

The influence on global warming of a second process, sea-ice changes, is more clear-cut. Sea-ice retreat with increasing CO₂ in the CSM is less than in the DOE model in spite of identical sea-ice formulations. As suggested in previous studies, some decrease of warming in the southern oceans, and thus less sea-ice response at high southern latitudes, could be expected from the inclusion of the GM mixing scheme in the CSM. Another factor that could reduce warming in the CSM in comparison with the DOE model is differences in the area-weighted (CSM) versus ice fraction threshold (DOE) ocean-atmosphere heat and moisture fluxes. Additionally, the systematic errors in the control integrations are not the same in the models, and this could lead to different climatic responses.

The difference in sea-ice area response between the two models is also a factor—probably the most important factor. A simple feedback analysis indicates that global warming would be reduced by 37% in the DOE model but only 20% in CSM if there were no snow-sea ice changes with increasing CO₂. Most of this response is associated with sea-ice changes as noted in previous studies. We therefore investigate the causes of the different sea-ice area responses in the two models in the Northern Hemisphere. These involve interactions between the ice, the surface energy balance, and ocean heat transport changes. To illustrate these processes, results from the Arctic region and the GIN Sea in particular are presented. The surface energy budget response is controlled primarily by surface albedo (in turn related to ice area changes) and cloud changes. In both models, increases in low cloud over the GIN Sea area partly

offset the effects of ice area changes. Because of this, the surface energy budget appears to play a relatively minor role in determining ice-area reduction. A more important factor is the poleward ocean heat transport, associated with changes in meridional overturning in the GIN Sea. Although the DOE model has a much larger weakening of the hemispheric overturning response, the CSM actually has a greater weakening response in the GIN Sea region. Thus, in the increased CO₂ case the transport of warmer water from the south into this region in the DOE model is greater in comparison with the CSM. This leads to a larger ice reduction in the DOE model, thus contributing to the enhanced global warming response in the DOE model in comparison with the CSM. Changes of heat transport in the GIN Sea are clearly model dependent, and further investigation of this response needs to be undertaken in other models.

Acknowledgments. The authors acknowledge all those who contributed to the testing and running the CSM and DOE models. The CSM transient CO₂ simulation was performed on an SX4 computer at an NEC facility in Japan under sponsorship from the Central Research Institute of Electric Power Industry (CRIEPI). The authors wish to thank NEC for its help in porting and optimizing the CSM, and CRIEPI for performing the simulation and providing the results. Drs. A. Kasahara and J. Hack of NCAR and Mr. S. Nishinomaya and Dr. K. Maruyama of CRIEPI arranged the collaboration, and Dr. L. Buja of NCAR coordinated the code port and simulation. Some of the equilibrium simulations with CCM3 used here were funded under the ACACIA program, with assistance from R. Folkert (KEMA) and G. Bates (NCAR). A portion of this study was supported by the Office of Biological and Environmental Research, U.S. Department of Energy, as part of its Climate Change Prediction Program.

APPENDIX

Transient versus Equilibrium Sensitivity in the CSM

The atmospheric component of the CSM (CCM3), based on an equilibrium $2 \times \text{CO}_2$ experiment with the nondynamic mixed layer ocean coupled to the CCM3, has a global mean climate sensitivity of about 2.1°C. The corresponding top-of-the-troposphere forcing, after stratospheric equilibration, is estimated to be 3.5 W m^{-2} . It is of interest to determine whether the 1% per year (compound) CO₂ increase run with the CSM gives a transient response that is consistent with this sensitivity.

In order to do this, one must somehow estimate the lag or damping effect of oceanic thermal inertia on the transient response. One method for accounting for lag effects in a controlled way is to use a simpler climate model in which sensitivity and lag-related parameters can be specified a priori. Here, we use the upwelling-

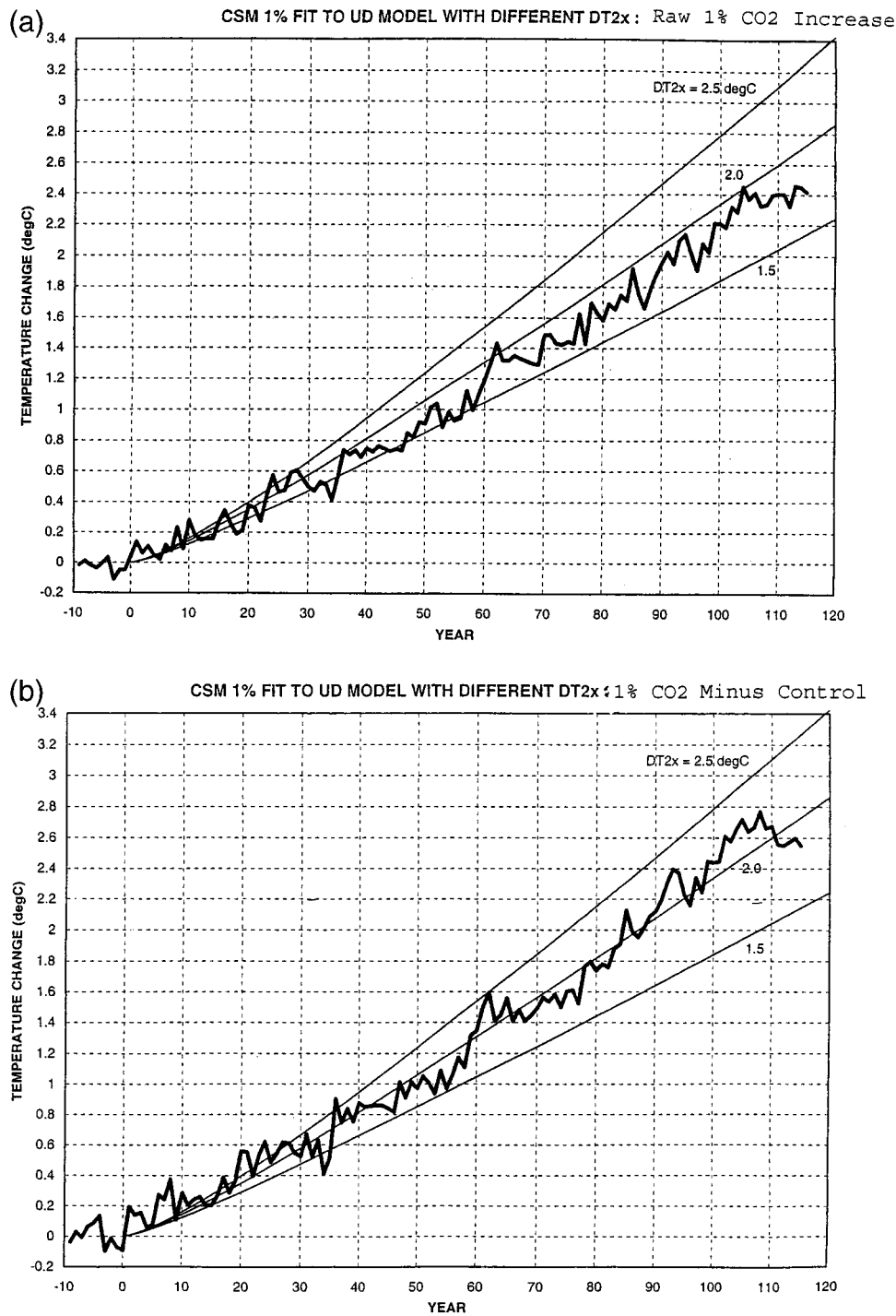


FIG. A1. (a) Raw CSM globally averaged temperature time series from the 1% yr⁻¹ CO₂ increase experiment (heavy line), and UD EBM model results for sensitivities of 1.5°, 2°, and 2.5°C; (b) same UD EBM results as in (a) but increased CO₂ minus control time series for the CSM.

diffusion energy-balance model (UD EBM) of Wigley and Raper (1992) and follow the procedure of Raper and Cubasch (1996) in their analysis of transient runs with the Max Planck Institute (MPI) global coupled model (ECHAM3/LSG). The UD EBM distinguishes

between land and ocean in each hemisphere, has differential (and adjustable) land–ocean climate sensitivity (see, e.g., Murphy 1995), and allows the meridional overturning (i.e., upwelling) rate to vary with time. Further details are given in Raper and Cubasch (1996).

To compare UD EBM results with the CSM 1% run, we use the same forcing history and model parameters as in Raper and Cubasch (1996), and a range of global climate sensitivity values. Also, in accord with the behavior of CSM, we keep the upwelling rate constant. If the 2.1°C sensitivity from CCM3 applies to CSM, then the UD EBM and CSM results should match when this sensitivity value is specified for the UD EBM. Note that a less-than-perfect match would not necessarily prove that CCM3 and the CSM had different sensitivities; it could point to differences between the UD EBM's simulation of oceanic inertia (lag) effects and those of the CSM.

In making our comparison, we have two choices for the CSM temperature data; we can either use the raw data, or we can consider the difference between the 1% run and the CSM control run. We consider both possibilities here.

Use of the 1% minus control difference requires an act of faith. Essentially this assumes that any low-frequency "drift" in the control will be echoed in the perturbed run. It is unclear how one could ever test this assumption. Raper and Cubasch (1996) conclude, for the MPI ocean-atmosphere general circulation model (O-AGCM), that this assumption is unlikely to be true. The MPI model, however, may be a special case because it has a very large drift in its control run, an order of magnitude or more greater than in the CSM. Instead of assuming comparable drifts in the two runs, a better way to look at the use of 1% minus control differences is as an assessment of the sensitivity of the UD EBM-O-AGCM comparison to possible drift (i.e., low-frequency changes unrelated to the applied forcing) in the O-AGCM perturbed run.

The results are shown in Fig. A1. Figure A1a compares the raw O-AGCM results with UD EBM results for sensitivities of 1.5°, 2.0°, and 2.5°C. (The first 10 yr of the O-AGCM results are a small "start-up" period prior to switching on the forcing. Both O-AGCM and UD EBM results are relative to the mean over the start-up period.) The best fit between the two models is for a sensitivity of around 1.8°C.

Figure A1b compares the same UD EBM results with the 1% minus control differences from the O-AGCM. Here, because the control shows a slight downward drift over the perturbed-run interval (see main text, Fig. 1a), difference values show a larger warming than for the raw perturbed-run data. The best match between the two models in this case is for a sensitivity of around 2.0°C, consistent with the equilibrium experiment result. Thus, it could be expected that, in spite of the different sea ice and SST base state, if the CSM were run to equilibrium with doubled CO₂, it would produce a global warming near 2°C, which is about the value from the slab ocean version run to equilibrium with doubled CO₂.

REFERENCES

- Bonan, G. B., 1998: The land surface climatology of the NCAR land surface model (LSM 1.0) coupled to the NCAR Community Climate Model (CCM3). *J. Climate*, **11**, 1307–1326.
- Bony, S., K.-M. Lau, and Y. C. Sud, 1997: Sea surface temperature and large-scale circulation influences on tropical greenhouse effect and cloud radiative forcing. *J. Climate*, **10**, 2055–2077.
- Boville, B. A., and P. R. Gent, 1998: The NCAR Climate System Model, version one. *J. Climate*, **11**, 1115–1130.
- Cane, M. A., A. C. Clement, A. Kaplan, Y. Kushnir, D. Pozdnyakov, R. Seager, S. E. Zebiak, and R. Murtugudde, 1997: Twentieth-century sea surface temperature trends. *Science*, **275**, 957–960.
- Cess, R. D., and Coauthors, 1996: Cloud feedback in atmospheric general circulation models: An update. *J. Geophys. Res.*, **101**, 12 791–12 794.
- Chou, M.-D., W. Zhao, and S.-H. Chou, 1998: Radiation budgets and cloud radiative forcing in the Pacific warm pool during TOGA COARE. *J. Geophys. Res.*, **103**, 16 967–16 977.
- Collins, M., 2000: The El Niño–Southern Oscillation in the second Hadley Centre coupled model and its response to greenhouse warming. *J. Climate*, **13**, 1299–1312.
- Dickinson, R. E., G. A. Meehl, and W. M. Washington, 1987: Ice-albedo feedback in a CO₂ doubling simulation. *Climatic Change*, **10**, 241–248.
- Gates, W. L., 1992: AMIP: The Atmospheric Model Intercomparison Project. *Bull. Amer. Meteor. Soc.*, **73**, 1962–1970.
- Gent, P., F. Bryan, G. Danabasoglu, S. Doney, W. Holland, W. Large, and J. McWilliams, 1998: The NCAR Climate System Model global ocean component. *J. Climate*, **11**, 1287–1306.
- Hack, J. J., 1998: Sensitivity of the simulated climate to a diagnostic formulation for cloud liquid water. *J. Climate*, **11**, 1497–1515.
- Jones, P. D., 1988: The influence of ENSO on global temperatures. *Climate Monit.*, **17**, 80–89.
- Kattenberg, A., and Coauthors, 1996: Climate models—Projection of future climate. *Climate Change 1995: The Science of Climate Change, IPCC Second Assessment Report*, J. T. Houghton et al., Eds., Cambridge University Press, 285–357.
- Kiehl, J. T., J. J. Hack, G. Bonan, B. Boville, B. P. Briegleb, D. Williamson, and P. Rasch, 1996: Description of the NCAR Community Climate Model (CCM3). NCAR Tech. Note NCAR/TN-420+STR, 152 pp. [Available from NCAR, P.O. Box 3000, Boulder, CO 80307.]
- , —, —, —, D. Williamson, and P. Rasch, 1998: The National Center for Atmospheric Research Community Climate Model (CCM3). *J. Climate*, **11**, 1131–1149.
- Kitoh, A., S. Yukimoto, A. Noda, and T. Motoi, 1997: Simulated changes in the Asian summer monsoon at times of increased atmospheric CO₂. *J. Meteor. Soc. Japan*, **75**, 1019–1031.
- Knutson, T. R., and S. Manabe, 1995: Time-mean response over the tropical Pacific due to increased CO₂ in a coupled ocean-atmosphere model. *J. Climate*, **8**, 2181–2199.
- , and —, 1998: Model assessment of decadal variability and trends in the tropical Pacific Ocean. *J. Climate*, **11**, 2273–2296.
- Levitus, S., 1982: *Climatological Atlas of the World Ocean*. National Oceanic and Atmospheric Administration, NOAA Professional Paper No. 13, 173 pp. and 17 microfiche. [Available from U.S. Government Printing Office, Washington, DC 20402.]
- Maruyama, K., H. Hirakuchi, J. Tsutsui, N. Nakashiki, S. Kadokura, and M. Kadoyu, 1997: Global warming projection for 125 years using NCAR CSM coupled model. CRIEPI Tech. Rep. U97834, Central Research Institute of Electric Power Industry, Tokyo, Japan, 24 pp. [Available from CRIEPI, 1646 Abiko Abiko-shi, Chiba 270-1194, Japan.]
- Meehl, G. A., 1996: Vulnerability of fresh water resources to climate change in the tropical Pacific region. *J. Water, Air Soil Pollut.*, **92**, 203–213.
- , 1997: Modification of surface fluxes from component models in global coupled models. *J. Climate*, **10**, 2811–2825.
- , and W. M. Washington, 1990: CO₂ climate sensitivity and snow–sea-ice albedo parameterization in an atmospheric GCM coupled to a mixed-layer ocean model. *Climatic Change*, **16**, 283–306.
- , and —, 1993: South Asian summer monsoon variability in

- a model with doubled atmospheric carbon dioxide concentration. *Science*, **260**, 1101–1104.
- , and —, 1995: Cloud albedo feedback and the super greenhouse effect in a global coupled GCM. *Climate Dyn.*, **11**, 399–411.
- , and —, 1996: El Niño-like climate change in a model with increased atmospheric CO₂ concentrations. *Nature*, **382**, 56–60.
- , and J. Arblaster, 1998: The Asian–Australian monsoon and El Niño–Southern Oscillation in the NCAR Climate System Model. *J. Climate*, **11**, 1357–1387.
- , G. W. Branstator, and W. M. Washington, 1993: Tropical Pacific interannual variability and CO₂ climate change. *J. Climate*, **6**, 42–63.
- , W. M. Washington, D. J. Erickson III, B. P. Briegleb, and P. J. Jaumann, 1996: Climate change from increased CO₂ and direct and indirect effects of sulfate aerosols. *Geophys. Res. Lett.*, **23**, 3755–3758.
- , G. J. Boer, C. Covey, M. Latif, and R. J. Stouffer, 1997: Intercomparison makes for a better climate model. *Eos, Trans. Amer. Geophys. Union*, **78**, 445–446, 451.
- , W. M. Washington, J. M. Arblaster, T. W. Bettge, and W. G. Strand, 2000: Anthropogenic forcing and decadal climate variability in sensitivity experiments of twentieth- and twenty-first-century climate. *J. Climate*, in press.
- Murphy, J. M., 1995: Transient response of the Hadley Centre coupled ocean–atmosphere model to increasing carbon dioxide. Part III: Analysis of global-mean response using simple models. *J. Climate*, **8**, 496–514.
- Nicholls, N., G. V. Gruza, J. Jouzel, T. R. Karl, L. A. Ogallo, and D. E. Parker, 1992: Observed climate variability and change. *Climate Change 1992: The Supplementary Report to the IPCC Scientific Assessment*, J. T. Houghton, B. A. Callander, and S. K. Varney, Eds., Cambridge University Press, 133–192.
- Power, S. B., and A. C. Hirst, 1997: Eddy parameterization and the oceanic response to idealized global warming. *Climate Dyn.*, **13**, 417–428.
- Raper, S. C. B., and U. Cubasch, 1996: Emulation of the results from a coupled general circulation model using a simple climate model. *Geophys. Res. Lett.*, **23**, 1107–1110.
- Rasch, P. J., and J. E. Kristjansson, 1998: A comparison of the CCM3 model climate using diagnosed and predicted condensate parameterizations. *J. Climate*, **11**, 1587–1614.
- Robock, A., 1983: Ice and snow feedbacks and the latitudinal and seasonal distribution of climate sensitivity. *J. Atmos. Sci.*, **40**, 986–997.
- Schlesinger, M. E., 1989: Quantitative analysis of feedbacks in climate model simulations. *Understanding Climate Change, Geophys. Monogr.*, No. 52, Amer. Geophys. Union, 177–187.
- Senior, C. A., 1999: Comparison of mechanisms of cloud-climate feedbacks in GCMs. *J. Climate*, **12**, 1480–1489.
- Spelman, M. J., and S. Manabe, 1984: Influence of oceanic heat transport upon the sensitivity of a model climate. *J. Geophys. Res.*, **89**, 571–586.
- Tett, S., 1995: Simulation of El Niño–Southern Oscillation-like variability in a global AOGCM and its response to CO₂ increase. *J. Climate*, **8**, 1473–1502.
- Timmermann, A., J. Oberhuber, A. Bacher, M. Esch, M. Latif, and E. Roeckner, 1999: Increased El Niño frequency in a climate model forced by future greenhouse warming. *Nature*, **398**, 694–697.
- Washington, W. M., and G. A. Meehl, 1984: Seasonal cycle experiment on the climate sensitivity due to a doubling of CO₂ with an atmospheric general circulation model coupled to a simple mixed layer ocean model. *J. Geophys. Res.*, **89**, 9475–9503.
- , and —, 1993: Greenhouse sensitivity experiments with penetrative cumulus convection and tropical cirrus albedo effects. *Climate Dyn.*, **8**, 211–223.
- , and —, 1996: High latitude climate change in a global coupled ocean–atmosphere–sea ice model with increased atmospheric CO₂. *J. Geophys. Res.*, **101**, 12 795–12 801.
- , and Coauthors, 2000: Parallel Climate Model (PCM) control and 1% per year CO₂ simulations with a 2/3 degree ocean model and a 27-km dynamical sea ice model. *Climate Dyn.*, in press.
- Weatherly, J. W., B. P. Briegleb, W. G. Large, and J. A. Maslanik, 1998: Sea ice and polar climate in the NCAR CSM. *J. Climate*, **11**, 1472–1486.
- Wigley, T. M. L., and S. C. B. Raper, 1992: Implications for climate and sea level of revised IPCC emissions scenarios. *Nature*, **357**, 293–300.